Memoirs of the Faculty of Science, Kyoto University, Series of Physics, Astrophysics, Geophysics and Chemistry, Vol. XXXIX, No. 2, Article 2, 1995

A Far-Infrared H-R Diagram of Young Stellar Objects

By

Thomas DJAMALUDDIN and Mamoru SAITŌ

Department of Astronomy, Faculty of Science, Kyoto University
Kyoto 606-01, Japan

(Received November 25, 1994)

Abstract

The observed spectral energy distributions of high- and low-mass young stellar objects (YSOs) are almost a modified blackbody-like one at far-infrared (FIR) to millimeter wavelengths. These emissions are produced at the outer envelopes of YSOs and the spectra are represented by the FIR color made by the *IRAS* flux densities at 60 and 100 μm, f_{60} and f_{100}. For the nearby star-forming regions in Per-OB2, Taurus, Orion, Vela, and ρ-Ophiucus molecular clouds, we selected cold *IRAS* point sources corresponding to YSOs by using the color criterion of $f_{60} > f_{12}$, and constructed FIR H-R diagrams of YSOs, i.e., the luminosity of 60 μm versus the color $\log(f_{100}/f_{60})$ relation. We also examined the visual counterparts of these YSOs on the POSS prints. The FIR H-R diagrams for the individual star-forming regions show common properties in the luminosity-color relation and the locations of the extreme Class I YSOs and the active YSOs. The fundamental line on the FIR H-R diagram is a *constant envelope mass sequence* (CEMS) along which YSOs move following the evolutionary change in the luminosity of the central object. From analysis of the FIR H-R diagrams, we suggest that the extreme Class I YSOs have already stored most of material of stellar mass in the central part and are forming stars through a slow accretion of the material.

1. Introduction

In a star forming molecular cloud, there are many young stellar objects (hereafter YSOs) with various masses in various evolutionary stages (e.g., Myers et al. 1987; Strom, Strom & Merrill 1993). Our knowledge about evolutionary process of YSOs is still incomplete in the sense that we do not know observational parameters specifying both the evolutionary stage of such YSOs and the resultant stellar mass which is the fundamental parameter of stars.

Hydrodynamical studies claim that molecular cores collaspe with increasing of luminosity, and the mass concentrated into the central part forms protostar and the surrounding disk (e.g., Larson 1977; Terebey, Shu & Cassen 1984; Shu, Adams & Lizano 1987). YSOs radiate mainly infrared emission with broad spectral energy distributions (SEDs) with the variety in extension shortward of mid-infrared wavelength; the emissions at mid- and near-infrared wavelengths come from the inner objects consisting of star and the surrounding disk and the SEDs spread towards shorter wavelengths with time, as the inner objects evolve and the outer envelope disperses (e.g., Wynn-Williams 1982; Chini, Krügel & Kreysa 1986; Adams, Lada & Shu 1987;

Lada 1987; Myers et al. 1987; Shu et al. 1987; Kenyon, Calvet & Hartmann 1993). The SEDs are thus considered to indicate evolutionary stages of YSOs; the indicators proposed so far are the slope between mid- and near-infrared wavelength (Lada 1987) and the mean frequency (Ladd et al. 1991).

It is recently recognized that the observed YSOs spectra from FIR to millimeter, i.e., the longer wavelength part of the broad SEDs, fit a modified blackbody radiation with a peak around 100 μm for both high- and low-mass YSOs (e.g., Beckwith et al. 1986; Chini et al. 1986; Davidson 1987; Wilking et al. 1989; Walker, Adams & Lada 1990, hereafter WAL; Ladd et al. 1991); that is, the flux densities are proportional to $\nu^{\beta} B_{\nu}(T)$, where $B_{\nu}(T)$ is the Planck function for a temperature $T \sim 20$ to 50 K and ν^{β} is proportional to a dust emissivity with $\beta \sim 1$ to 2. WAL interpret the observed spectra of 12 star-forming molecular cores by a model of isothermal dusty envelopes, by adopting probable values of three parameters, T ($\simeq$25 to 61 K), β ($\simeq$0.87 to 1.79), and apparent size. Figure 1 shows that the WAL's temperatures of 11 objects, for which WAL performed the fitting for the spectra measured at 56 to 3,350 μm, are correlated with the color $[100\text{–}60] \equiv \log(f_{100}/f_{60})$ for the *IRAS* flux densities at 100 μm and 60 μm and the color temperatures for $\beta = 1$. Figure 1 suggests that the *IRAS* color [100–60] represents some average temperature of the outer envelope of YSOs (Ellis et al. 1990).

When a dust grain in optically thin envelope of YSOs is illuminated by radiation from the central objects, its temperature, T_d, depends mainly on the luminosity, L_*, of the central objects and radius, r, of envelope as

$$T_d = [L_* T_*^{\beta} / (16\pi\sigma r^2)]^{1/(4+\beta)}, \tag{1}$$

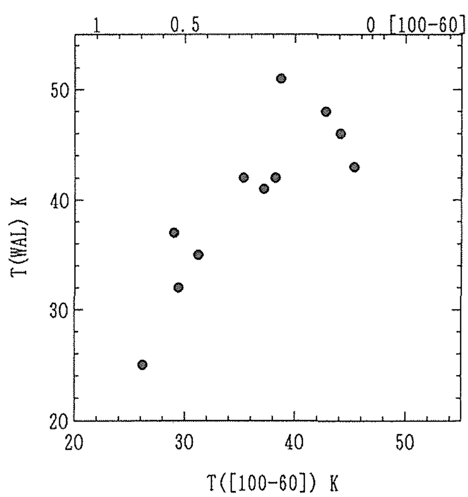

Fig. 1. Color temperatures of YSOs, $T_{100/60}$, derived from *IRAS* flux densities at 60 μm and 100 μm versus dust temperatures, T_{WAL}, derived by Walker, Adams & Lada (1990). The flux density of dust emission is assumed to be proportional to $\nu^{\beta} B_{\nu}(T)$, where B_{ν} is the Planck function and β is a constant. The color temperatures are derived for $\beta = 1$, while T_{WAL} were derived for fitting of the spectra measured at wavelengths of 58 to 3,350 μm, in which the values of β and dust temperature are free parameters.

where β is a constant in dust emissivity of $\propto \nu^{\beta}$ and the value is 1 to 2 (Hildebrand 1983), T_* is the effective temperature of the central object, and σ is the Stefan-Boltzmann constant (Scoville & Kwan 1976; Beckwith et al. 1986). During the collapsing phase, L_* remarkably increases with time, while the radius of outer envelope is nearly constant (e.g., Shu 1977; Terebey et al. 1984). Therefore, evolution of a YSO in the collapsing phase may be traced by a locus on $T_d - L_*$ plane, along which T_d and L_* both become higher with time. The values of L_* and r both are larger for higher-mass YSOs and the loci of YSOs on the $T_d - L_*$ plane separate with YSOs' mass.

Numerical caluculations of radiative transfer in spherical, dusty protostellar envelopes were carried out by Scoville & Kwan (1976), Rowan-Robinson (1980), Yorke (1980), Yorke & Shustov (1981), Adams & Shu (1985), Gürtler et al. (1991), Kenyon et al. (1993), and others. The main parameters are stellar (or central object) mass and luminosity, dust properties, and mass and density distribution of envelope. The resulting spectra in FIR to millimeter wavelengths are similar for probable values of these parameters and always show a peak at FIR. The slopes of SEDs at $\sim 100\ \mu$m to 1 mm correspond to those for $\beta \sim 1$ (Yorke & Shustov 1981), and the color temperatures do not change at 50 to $100\ \mu$m with wavelength and thus the spectra look like a blackbody in spite of optically thin envelopes at these wavelengths (Rowan-Robinson 1980). These features are consistent with the above-mentioned observed features. As the envelope mass is less, the FIR peak moves toward shorter wavelength (Yorke 1980; Kenyon et al. 1993). If the envelope mass is fixed and the luminosity increases, the FIR peak moves also toward shorter wavelength (Kenyon et al. 1993). The effective radius at FIR does not change with time during the evolutionary phase with optical depth of 1,000 to 10 at $0.1\ \mu$m (Yorke & Shustov 1981). Based on the radiative transfer calculations, Chini et al. (1986), Churchwell, Wolfire & Wood (1990), and Kenyon et al. (1993) found the structures of the envelope and central disk reproducing the observed SEDs.

These observed and calculated spectral features of YSOs at FIR suggest that a FIR H-R diagram of YSOs may describe early phase of evolution of YSOs, although any H-R diagram has been considered to be impossible (Beichman et al. 1986; Adams 1990; Lada 1991; Myers & Ladd 1993). In this paper we propose a FIR H-R diagram of YSOs for each star-forming region by using *IRAS* flux densities at $60\ \mu$m and $100\ \mu$m; the color is $[100\text{–}60] \equiv \log(f_{100}/f_{60})$ and the luminosity is $L_{60} \equiv d^2 f_{60}$, where d is the distance to the star forming region. The reasons that we use these parameters are as follows:

(1) The emissions at $60\ \mu$m and $100\ \mu$m originate at almost the same region in outer envelope of a YSO; the envelope extends outside a near-infrared photosphere surrounding the central objects (e.g., Stahler, Shu & Taam 1980) and the color [100–60] represents some average dust temperature at the envelope (e.g., Chini et al. 1986; Butner et al. 1990; Ellis et al. 1990). We call the region the FIR emitting envelope. Note that the color temperature corresponding to [100–60] follows a change of a total luminosity of YSO (see equation (1)), rather than the FIR luminosity which depends on dust mass in the envelope as well as its dust temperature.

(2) The FIR emitting envelope is optically thin at 60 μm and 100 μm (e.g. Harvey et al. 1979; Kenyon et al. 1993; Natta et al. 1993), and thus its fluxes are independent on the geometry of YSOs, although the observed features in near-infrared wavelength depend on the geometry.

(3) The flux densities at 60 μm is more free from diffuse component than those at 100 μm, and sensitively change with dust temperature because 60 μm tends to be at the side of the Wien distribution of the modified blackbody-like SEDs.

(4) *IRAS* provides us unbiased survey data of YSOs in almost all nearby star-forming regions.

In §2 we construct FIR H-R diagrams of YSOs for nearby star-forming regions and describe properties of the FIR H-R diagrams. In §3 we discuss mass of the FIR emitting envelope and an evolutionary track of YSOs on the FIR H-R diagram. A summary is given §4.

2. Far-Infrared H-R Diagrams of YSOs

2.1. Selection of Star-Forming Regions and Cold IRAS Point Sources

YSOs are detected as cold *IRAS* point sources in star-forming regions (Beichman et al. 1986; Wood & Churchwell 1989). In a star-forming region, YSOs form in some mass range and time span under similar environment. We thus consider that a FIR H-R diagram for *each* star-forming region contains essential information of evolution of YSOs. We here treat six well-known, nearby star forming regions in Perseus-OB2, Taurus, Orion A and B, Vela, and ρ-Ophiuchus molecular clouds; these are within 700 pc in distance and each contains 50 or more cold *IRAS* point sources.

We define *cold IRAS* point sources in *IRAS* Point Source Catalog (*IRAS PSC*) using the flux densities at 12 and 60 μm; the color criterion is $f_{12}<f_{60}$ and the source is so bright that f_{60} has good or moderate flux quality ($FQ_{60}\geq 2$). The color criterion selects all kinds of YSOs such as T Tauri stars with residual envelope, massive YSOs with compact H II region, and other YSOs embedded in molecular cloud cores (e.g., Beichman et al. 1986; Emerson 1987; Harris, Clegg & Hughes 1988; Wilking, Lada & Young 1989; Wood & Churchwell 1989). We chose the cold *IRAS* point sources still located on the parent CO clouds. We also made a visual search for optical counterparts of the selected sources on the *POSS* prints; the procedure is similar with Yamada et al. (1993) in searching for *IRAS* galaxies. If a source is associated with a galaxy or a planetary nebula in our visual inspection or if the association with non-YSOs, including main-sequence star, is denoted in literature, we omit it from our sample.

The upper limit, 2′, in size of *IRAS* point sources at 100 μm (*IRAS* Explanatory Supplement 1988) corresponds to 0.1 pc at the nearest star forming regions in Taurus and ρ-Ophiuchus where low-mass stars are forming. The sizes of extended components of YSOs and T-Tauri stars in these regions have been measured using molecular lines and millimeter continuum, and they are smaller than 0.02 pc (e.g., André et al. 1990; Ohashi et al. 1991). The radius of the FIR emitting region derived from equation (1) is $4.3\times10^{-4}(T_*/T_d)^{\beta/2}(30/T_d)^2(L_{IR}/L_\odot)^{1/2}$ pc; for $T_d=20-50$ K, $T_*=300-600$ K, and $\beta=1-2$, the radius is almost less than 0.1 pc for $L_{IR}<20L_\odot$.

Thus isolated YSOs brighter than the sensitivity limit of *IRAS* observations are detected as *IRAS* point sources, and some confused sources may be identified as extended sources. At the Orion molecular clouds whose distance is about 500 pc, the critical size of *IRAS* point sources is 0.3 pc and it is comparable to the typical diameters of CS($J=2-1$) molecular cores (Lada, Bally & Stark 1991 ; Tatematsu et al. 1993). The radius of the FIR emitting region is less than 0.3 pc for $L_{IR}<200L_{\odot}$. Most of YSOs in Orion are thus identified as *IRAS* point sources. The brighest infrared sources OMC1 and OMC2 in Orion A are, respectively, an *IRAS* extended source and an *IRAS* point source with an upper limit flux density at 60 μm and are not contained in our objects. These are complexes of two or more YSOs (Mezger, Wink & Zylka 1990). The Vela star forming region is at 700 pc (Liseau et al. 1992).

The most luminous infrared sources in each star forming region often correspond to clustering of YSOs where the projected surface densities of YSOs are up to ~ 100 pc^{-2} (e.g., Lada et al. 1991 b ; Strom et al. 1993; Carpenter et al. 1993). Some of these objects are identified as *IRAS* extended sources, such as OMC1. The beam size of *IRAS* observations at 100 μm is 0.3 pc at the Orion and 0.4 pc at the Vela, and it is still possible that some brightest *IRAS* point sources selected are the complexes of several or more YSOs. We examine the complexness of such *IRAS* point sources by using *IRAS PSC* and literature.

The selected star-forming regions are summarized in Table 1 as well as the adopted extents in Galactic coordinate and the numbers of the selected *IRAS* point sources. The sky distributions of the selected sources are shown in Figure 2. In order to avoid contamination by objects in adjacent star-forming regions, we restricted the range of

Table 1. The Selected Star-Forming Regions and Number of Cold *IRAS* Point Sources

Name	Galatic coordinate		Area (deg^2)	$d^{1)}$ (kpc)	Number$^{2)}$	Density (deg^{-2})
	l_{min}, l_{max}	b_{min}, b_{max}				
PER-OB2	156, 162	−24, −16	9.6	0.35	84 (8 : 27 : 8 : 41)	8.8
TAURUS	169, 177	−19, −12	36.2	0.14	54 (19 : 19 : 12 : 4)	1.5
ORION B	204, 209	−17.5, −12.5	13.5	0.5	89 (15 : 19 : 19 : 36)	6.7
ORION A	205, 215	−21, −17.5	24.3	0.5	147 (30 : 29 : 40 : 48)	6.0
VELA	260, 266	−0.5, 3	16.3	0.7	179 (42 : 38 : 38 : 61)	11.0
ρ-Oph	351, 359	12, 20	17	0.125	84 (4 : 25 : 12 : 43)	5.0

1) The distances are adopted following Ungerechts and Thaddeus (1987) for Per-OB2 and Taurus, Maddalena et al. (1986) for Orion A and B, Liseau et al. (1992) for Vela, and de Geus, Bronfman, and Thaddeus (1990) for ρ-Ophiucus. 2) Total number of the selected sources with $f_{60}>f_{12}$ and good or moderate flux quality at 60 μm, $FQ_{60}\geq 2$; these are classified into four groups based on the flux quality at 12 and 100 μm, i.e. (FQ_{100}, FQ_{12})=($\geq$2, $\geq$2), ($\geq$2, 1), (1, $\geq$2), and (1, 1). The numbers of the sources for four groups are denoted in parenthesis.

each star-forming region within the area where there is a single molecular cloud in the line of sight (Sargent 1979; Dame et al. 1987; Maddalena et al. 1986; Ungerechts & Thaddeus 1987; Wouterloot & Brand 1989; de Geus, Bronfman & Thaddeus 1990).

We list the data of the individual *IRAS* point sources in Table 2. The *IRAS* point sources are divided into two groups in each star-forming region by the flux quality at 100 μm, FQ_{100}; the first group is for $FQ_{100} \geq 2$ and the second for $FQ_{100} = 1$. In the present paper we use mainly the data of the first group. The data of the second group are listed for more complete study in future. All of the *IRAS* data are taken from *IRAS PSC*. The parameters in Table 2 are as follows:

Column 1: *IRAS* name.

Columns 2 and 3: Galactic coordinate which is transformed from the equatorial coordinate of *IRAS PSC*.

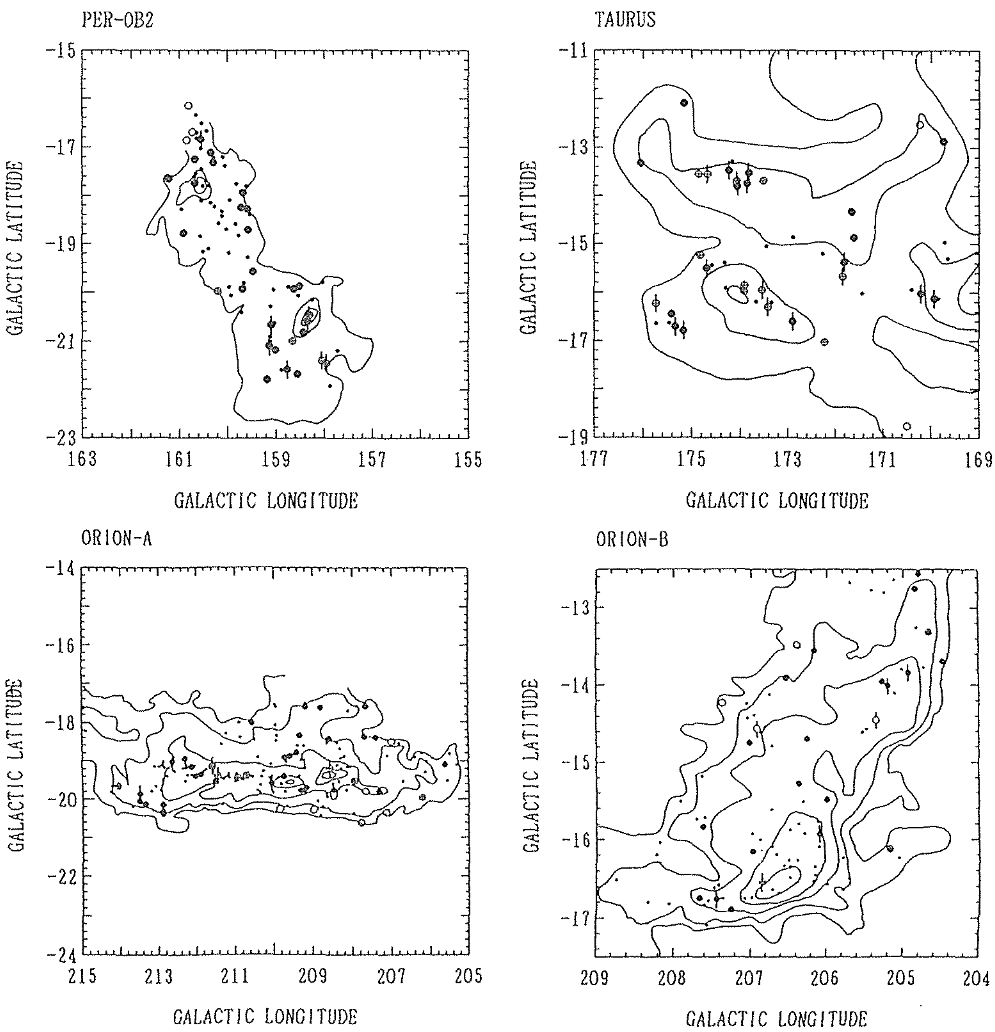

Fig. 2

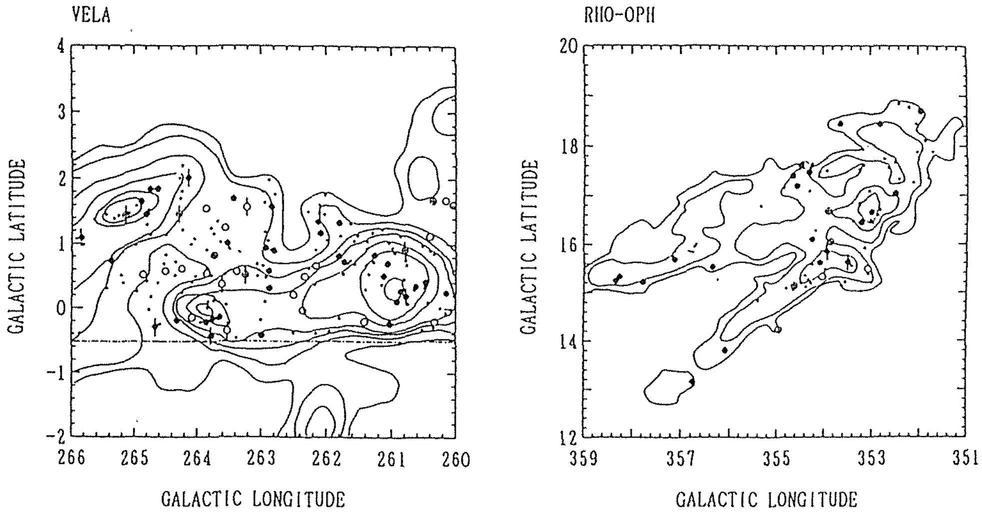

Fig. 2. Sky distribution of all of the selected *IRAS* point sources (i.e., cold YSOs) in the six nearby star-forming clouds. The filled circles are invisible sources, the circles with cross are sources with visible stars, and the open circles are sources whose optical counterparts are uncertain; all of these sources have reliable flux densities at 60 and 100 μm. The small dots are sources with upper limits of the flux densities at 100 μm, and are not used in the FIR H-R diagrams of Figure 3. The vertical bars indicate that the sources show some active features such as molecular outflow, H_2O maser, and H II region. The contours indicate the ^{12}CO intensity following Sargent (1979) for Per-OB2, Dame et al. (1987) for Taurus and Vela, Maddalena et al. (1986) for Orion A and B, and de Geus et al. (1990) for ρ-Ophiuchus. The outermost contours indicate the antenna temperature of 2.5 K for Per-OB2, the intensity of 5 K km s^{-1} for Taurus, Vela and ρ-Ophiuchus, and 1.28 K km s^{-1} for Orion A and B.

Column 4: Flux qualities (FQ) for *IRAS* four bands in order of 12, 25, 60, and 100 μm; 1=upper limit, 2=moderate quality, and 3=high quality. The values of columns 5 to 10 are obtained even in the cases of $FQ_\lambda=1$ by using the upper limit values.

Column 5: Color [60–12] defined by $\log(f_{60}/f_{12})$, where f_λ is the color-corrected flux density at λ μm (*IRAS* Explanatory Supplement). We define cold *IRAS* point sources by this color so that the values are positive for the original values of f_{12} and f_{60} in *IRAS PSC*.

Column 6: The upper is color [100–60] defined by $\log(f_{100}/f_{60})$, which is used as a parameter of the FIR H-R diagram. The color-corrected flux densities are used. The lower is dust (color) temperature derived by equation (Emerson 1988 a),

$$T_d=\frac{41.66}{[100\text{–}60]+0.222(\beta+3)} \tag{2}$$

for $\beta=1$. The value is denoted for the first group only.

Column 7: Uncertainty of the color [100–60], calculated from the uncertainties of f_{60} and f_{100}. This column is blank for the second group.

Column 8: The upper is logarithm of the luminosity at 60 μm defined by $L_{60}=d^2 f_{60}$, where d is distance in kpc to the star forming region (see Table 1) and f_{60} is the color-corrected flux density in Jy. $\log L_{60}$ is related with logarithm of the

Table 2. Cold *IRAS* Point Sources on the Six Nearby Star-Forming Regions

IRAS NAME (1)	l (2)	b (3)	FQ (4)	60-12 (5)	100-60 Td (6)	Unc. (7)	logL60 logLf (8)	Unc. (9)	Lf/Lm logMenv (10)	OC (11)	SED (12)	Activity (13)	Other Name, Comments (14)	References (15)
<PER-OB2>														
03220+3035	157.947	-21.453	3322	0.64	0.38 33	0.09	-0.30 0.13	0.04	0.9 -1.31	2T	1	O,H2O	RNO13, L1448-IRS1	2,7,13,17
03225+3034	158.041	-21.410	3323	1.55	0.85 24	0.15	0.45 1.19	0.09	7.9 0.62	2	1	O,H2O,HII	L1448-IRS3, B-ZAMS	7,17,18,26
03235+3004	158.550	-21.678	1333	1.22	0.22 38	0.08	-0.28 0.08	0.03	>3.4 -1.69	1	1			7
03245+3002	158.768	-21.577	1333	2.26	0.29 35	0.14	0.77 1.16	0.04	>12.3 -0.46	1	1	O,H2O,HII	RNO15 FIR	7,13,18
03253+2938	159.181	-21.798	1123	0.44	1.00 22	0.10	-1.11 -0.24	0.05	>2.1 -0.57	1				
03254+3050	158.424	-20.819	3332	1.00	0.22 38	0.13	-0.26 0.10	0.04	1.5 -1.67	1	1			7
03257+3034	158.648	-20.991	3333	0.15	0.93 23	0.09	-1.09 -0.28	0.03	1.0 -0.72	2T	2		LkH-α 325	2
03258+3104	158.341	-20.588	1133	2.91	0.36 33	0.11	1.37 1.79	0.05	>22.0 0.31	1		O,H2O	HH7-11(B)	19,36
03260+3111	158.304	-20.462	3333	1.15	0.24 37	0.07	1.82 2.19	0.02	2.7 0.46	2	1	HII	SVS 3, B-ZAMS	7,28
03265+3014	159.002	-21.173	1132	0.27	1.00 22	0.08	-1.26 -0.39	0.04	>1.4 -0.72	1				
03271+3013	159.129	-21.093	1332	1.43	0.04 45	0.09	-0.04 0.27	0.04	>2.7 -1.90	1	1	O		7,22
03282+3035	159.093	-20.665	1133	0.98	0.79 25	0.08	-0.57 0.12	0.03	>5.0 -0.55	1		O		22
03284+3132	158.514	-19.878	1123	0.38	0.98 22	0.09	-1.17 -0.31	0.05	>1.8 -0.68	1				
03287+3126	158.619	-19.921	1133	0.54	0.92 23	0.08	-1.01 -0.21	0.03	>2.2 -0.67	1				
03323+3049	159.682	-19.931	1132	0.47	1.18 20	0.11	-1.08 -0.05	0.05	>3.4 -0.09	1				
03326+3113	159.473	-19.572	1123	0.56	0.79 25	0.13	-1.00 -0.30	0.04	>1.9 -0.98	1				
03339+3029	160.188	-19.982	1332	1.05	-0.18 59	0.10	-0.20 0.09	0.04	>1.9 -2.61	2				
03355+3150	159.574	-18.711	1123	0.98	0.56 29	0.12	-0.58 -0.05	0.07	>3.3 -1.14	1				
03363+3207	159.530	-18.392	1132	0.99	0.72 26	0.20	-0.53 0.12	0.11	>4.2 -0.69	1				
03368+3210	159.588	-18.283	1132	0.89	0.54 29	0.14	-0.64 -0.12	0.07	>2.6 -1.25	1				
03373+3207	159.713	-18.254	1132	0.90	0.51 30	0.12	-0.65 -0.15	0.04	>2.6 -1.33	1				
03381+3223	159.675	-17.946	1132	0.73	0.86 24	0.10	-0.81 -0.05	0.05	>3.0 -0.62	1				
03382+3145	160.110	-18.426	2323	1.76	0.54 29	0.17	0.45 0.97	0.08	15.4 -0.16	1	1			7
03393+3148	160.263	-18.245	1123	0.98	0.88 24	0.16	-0.56 0.21	0.07	>5.7 -0.32	1				
03399+3059	160.913	-18.784	1123	0.93	0.81 25	0.12	-0.60 0.11	0.05	>4.3 -0.53	1				
03421+3229	160.290	-17.324	1123	0.58	0.88 24	0.11	-0.97 -0.19	0.04	>2.3 -0.73	1				
03422+3156	160.666	-17.746	1223	0.61	0.90 23	0.12	-0.74 0.05	0.06	>2.5 -0.45	1	1			7

Table 2. (Continued)

IRAS NAME (1)	l (2)	b (3)	FQ (4)	60-12 (5)	100-60 Td (6)	Unc. (7)	logL60 logLf (8)	Unc. (9)	Lf/Lm logMenv (10)	OC (11)	SED (12)	Activity (13)	Other Name,Comments (14)	References (15)
03429+3237	160.335	-17.121	1133	0.34	1.05 22	0.13	-1.18 -0.26	0.04	>1.8 -0.51	1				
03437+3219	160.670	-17.252	1133	0.81	0.64 27	0.10	-0.74 -0.15	0.07	>2.6 -1.10	1				
03444+3140	161.225	-17.650	1123	0.43	0.79 25	0.12	-1.10 -0.40	0.07	>1.4 -1.08	1				
03445+3242	160.547	-16.844	3333	0.94	0.01 46	0.06	0.26 0.57	0.02	1.4 -1.67	1	1	0	B5-IRS1, IR Neb.	7,15,31
03454+3230	160.836	-16.866	1133	0.47	0.94 23	0.06	-1.07 -0.25	0.03	>2.0 -0.68	3				
03455+3242	160.717	-16.700	1132	0.42	0.91 23	0.07	-1.12 -0.32	0.03	>1.7 -0.80	3				
03475+3304	160.806	-16.157	1133	0.28	0.99 22	0.07	-1.26 -0.40	0.04	>1.4 -0.74	3				
03205+3015	157.875	-21.922	1131	0.23	0.69		-1.23			3				
03219+3056	157.713	-21.193	1331	0.44	1.08		-1.05			1				
03222+3034	158.000	-21.441	1331	1.64	1.12		0.15			1	1		L1448-IRS2	7
03249+2957	158.887	-21.596	1131	0.35	1.07		-1.15			1				
03259+3105	158.346	-20.555	3331	1.28	0.61		1.45		<4.9	2E	1	O,H2O	HH7-11(A), SSV13	2,7,13,18
03262+3114	158.304	-20.404	3331	1.17	1.02		1.02		<12.0	1	1		BD +30°549	7
03267+3128	158.245	-20.147	1131	0.90	0.75		-0.66			1				
03270+3152	158.038	-19.799	1131	0.67	0.36		-0.86			1				
03273+3018	159.112	-21.009	1131	0.65	0.72		-0.80			1				
03276+3022	159.123	-20.908	1331	0.51	0.81		-0.82			2T	2		LkH-α 326	2,7
03279+3123	158.526	-20.061	1131	0.46	1.24		-1.09			1				
03281+3039	159.029	-20.621	1331	0.06	1.43		-1.26			1				
03292+3124	158.741	-19.884	1131	0.36	0.85		-1.17			1				
03293+3052	159.108	-20.289	1131	0.61	0.93		-0.83			1				
03301+3111	159.043	-19.942	3331	0.50	0.73		-0.21		<1.2	1	1	O		7
03310+3026	159.708	-20.410	1131	0.38	0.88		-1.13			2				
03326+3055	159.666	-19.813	1131	0.44	1.11		-1.02			1				
03328+3035	159.917	-20.063	1131	0.69	0.73		-0.87			1				
03334+3042	159.960	-19.888	1131	0.24	1.41		-1.27			1				
03338+3123	159.579	-19.283	1131	0.53	1.02		-1.03			1				
03354+3114	159.961	-19.192	1131	0.83	0.93		-0.65			1				
03358+3138	159.759	-18.831	1131	0.80	1.20		-0.75			1				
03367+3147	159.829	-18.591	1331	1.56	0.30		0.08			1	1			7
03371+3103	160.390	-19.112	1131	0.81	1.00		-0.66			1				
03371+3135	160.022	-18.698	1131	0.72	1.22		-0.79			1				
03374+3056	160.502	-19.169	1131	0.75	1.08		-0.74			1				
03380+3135	160.183	-18.587	1321	0.74	1.13		-0.67			2	2			7
03383+3232	159.599	-17.805	1131	0.47	1.07		-0.98			1				
03385+3109	160.555	-18.849	2321	1.14	0.94		-0.31		<8.6	1	1			7
03385+3149	160.109	-18.336	1231	0.73	1.56		-0.64			1	1			7
03386+3206	159.941	-18.094	1131	0.71	0.88		-0.79			1				
03391+3227	159.803	-17.759	1131	0.13	1.36		-1.15			1				
03398+3149	160.342	-18.160	3331	1.09	0.87		-0.07		<7.6	1	1			7
03406+3144	160.541	-18.116	1131	0.36	1.42		-0.91			1				
03410+3204	160.376	-17.799	3321	1.00	0.34		0.08		<2.6	1	1			7
03411+3235	160.050	-17.383	1131	0.52	1.16		-0.99			1				
03414+3200	160.501	-17.802	3321	2.10	0.43		1.35		<15.5	3				
03415+3121	160.951	-18.290	1131	0.57	0.80		-0.93			1				
03418+3242	160.088	-17.202	1131	0.23	1.47		-1.25			1				
03424+3234	160.280	-17.225	1131	0.31	1.39		-1.17			1				

Table 2. (Continued)

IRAS NAME (1)	l (2)	b (3)	FQ (4)	60-12 (5)	100-60 Td (6)	Unc. (7)	logL60 logLf (8)	Unc. (9)	Lf/Lm logMenv (10)	OC (11)	SED (12)	Activity (13)	Other Name, Comments (14)	References (15)
03426+3201	160.690	-17.622	1131	0.51	1.29		-1.04			1				
03426+3214	160.538	-17.451	3331	1.09	0.73		0.10		<3.5	2T				2
03427+3206	160.656	-17.546	1131	0.28	1.94		-1.22			1				
03439+3233	160.544	-17.033	1331	0.53	0.99		-0.89			1	1	0	B5 IRS3	8,13
03446+3254	160.422	-16.677	1331	0.30	1.34		-1.20			2	1			8
03449+3240	160.634	-16.822	1131	0.27	1.48		-1.28			1				
03452+3245	160.623	-16.709	1131	0.13	1.48		-1.30			1				
03454+3257	160.542	-16.522	1131	0.62	1.12		-0.93			1				
03464+3301	160.650	-16.347	1131	0.35	1.46		-1.18			1				
<TAURUS>														
04101+2450	170.492	-18.760	1132	0.54	0.33 34	0.10	-1.79 -1.39	0.03	>0.9 -2.92	3				
04169+2702	169.917	-16.129	3333	1.31	0.02 46	0.09	-0.49 -0.18	0.04	2.0 -2.40	1	1	0	IR Neb.	6,24,36
04181+2655	170.205	-16.023	2223	1.32	0.24 37	0.12	-0.93 -0.56	0.07	4.1 -2.29	1	1	0:	IR Neb.	6,24,36
04200+2759	169.705	-14.973	1222	0.27	0.29 35	0.19	-1.87 -1.48	0.04	>0.5 -3.10	3				
04206+2449	172.216	-17.021	3333	0.30	0.34 34	0.10	-1.76 -1.35	0.04	0.5 -2.87	2T			FT Tau	2
04239+2436	172.896	-16.607	3332	0.91	0.03 45	0.10	-0.54 -0.23	0.04	1.1 -2.42	1	1	0	IR Neb.	8,24,36
04240+2559	171.842	-15.675	3333	0.61	0.08 43	0.09	-0.12 0.20	0.05	0.8 -1.88	2T	2	0	DG Tau	2,10,24
04248+2612	171.809	-15.382	1333	1.09	0.29 35	0.07	-1.03 -0.64	0.03	>2.1 -2.26	1	1	0	B217,HH 31 IRS2,Neb.	8,24,36
04260+2642	171.598	-14.863	1232	0.63	0.22 38	0.11	-1.71 -1.35	0.03	>1.0 -3.12	1				
04263+2426	173.416	-16.307	3333	0.56	-0.08 52	0.15	0.04 0.34	0.06	0.6 -2.12	2T:	1	0	HARO 6-10, IR Mult.	2,8,13,32
04272+2923	169.734	-12.872	1133	0.63	0.71 26	0.10	-1.72 -1.08	0.03	>1.9 -1.90	1				
04278+2435	173.530	-15.955	3333	0.64	0.11 42	0.08	-1.18 -0.85	0.04	0.9 -2.86	2T	2	0	ZZ Tau	2,10,13
04279+2701	171.655	-14.331	1123	0.27	0.85 24	0.09	-2.06 -1.32	0.05	>1.1 -1.89	1				
04288+2417	173.909	-15.980	3333	0.88	0.34 34	0.10	-1.29 -0.88	0.03	1.5 -2.40	2T	2		HK Tau, IR Mult.	2,10,33
04292+2422	173.910	-15.858	3333	0.80	0.14 41	0.08	-0.85 -0.52	0.04	1.0 -2.46	2	2		Haro 6-13	2,8
04295+2251	175.166	-16.796	3332	0.76	0.31 35	0.09	-1.15 -0.75	0.04	1.1 -2.33	1	1	0		8,24
04299+2915	170.233	-12.521	1333	1.45	0.41 32	0.13	-0.56 -0.12	0.03	>6.1 -1.49	3	2D			6
04302+2247	175.336	-16.709	1333	1.42	0.17 39	0.09	-0.90 -0.55	0.04	>5.4 -2.43	1	1	0	IR Neb.	6,24,36
04313+2254	175.405	-16.452	1123	0.22	0.85 24	0.09	-2.11 -1.37	0.04	>0.9 -1.94	1				
04325+2402	174.689	-15.507	1333	1.69	0.23 37	0.10	-0.59 -0.22	0.03	>4.7 -1.97	1	1	0	L1535, IR Neb.	13,11,36
04328+2248	175.723	-16.238	3333	0.63	0.28 36	0.12	-0.77 -0.38	0.04	1.0 -2.03	2T	2D	0	HP Tau,(HBC414,415)	2,10,24
04337+2407	174.815	-15.234	1132	0.34	1.30 19	0.12	-2.01 -0.86	0.05	>3.3 -0.72	2				

Table 2. (Continued)

IRAS NAME (1)	l (2)	b (3)	FQ (4)	60-12 (5)	100-60 Td (6)	Unc. (7)	logL60 logLf (8)	Unc. (9)	Lf/Lm logMenv (10)	OC (11)	SED (12)	Activity (13)	Other Name, Comments (14)	References (15)
04353+2604	173.512	-13.689	3333	0.48	0.05 44	0.08	-0.94 -0.63	0.04	0.6 -2.77	2T	2		DO Tau	2,10
04361+2547	173.853	-13.746	3333	1.33	-0.08 52	0.10	-0.09 0.21	0.05	1.5 -2.25	1	1	0,H2O	TMR-1, IR Neb.	6,17,24,36
04365+2535	174.059	-13.808	3333	1.44	0.05 44	0.11	-0.16 0.15	0.05	2.6 -1.99	1	1	0	TMC1A, IR Neb.	8,24,36
04368+2557	173.823	-13.526	1333	1.83	0.61 28	0.10	-0.46 0.11	0.03	>19.5 -0.89	1	1	0	L1527, IR Neb.	6,11,24,36
04369+2539	174.073	-13.703	3332	0.19	0.39 33	0.10	-0.84 -0.40	0.04	0.4 -1.82	2T:	2	0	IC2087, IR Neb.	2,6,13
04381+2540	174.234	-13.477	3333	1.33	0.13 41	0.08	-0.69 -0.36	0.03	2.4 -2.32	1	1	0	TMC1, IR Neb.	8,24,36
04390+2517	174.681	-13.561	3333	0.40	0.70 26	0.12	-1.53 -0.90	0.04	1.1 -1.74	2T	2	0	V995 Tau,HBC422,423	2,10,24
04395+2509	174.855	-13.556	3323	0.12	0.55 29	0.09	-1.80 -1.28	0.04	0.4 -2.38	2T	2		DP Tau	2,10
04435+2424	176.041	-13.329	1123	0.23	1.08 21	0.09	-2.11 -1.17	0.04	>1.5 -1.37	1				
04454+2551	175.157	-12.098	1133	0.46	0.48 30	0.10	-1.85 -1.36	0.04	>0.8 -2.61	1				
04166+2706	169.828	-16.132	1331	1.29	0.54		-1.01			1	1			6
04181+2654	170.217	-16.033	2321	1.14	0.23		-1.01		<2.4	1	1			6
04188+2748	169.646	-15.306	3331	0.38	0.05		-1.66		<0.5	2T	2		DE Tau	2,10
04189+2650	170.395	-15.939	3331	0.67	0.19		-0.86		<0.9	2T			FS Tau & Haro6-5b	2
04216+2603	171.427	-16.016	1331	0.50	0.36		-1.72			3				
04264+2433	173.342	-16.213	3331	1.06	0.22		-0.97		<1.3	1	1			6
04267+2600	172.264	-15.201	3331	0.31	0.34		-1.79		<0.5	2wT	2		IQ Tau	2,10
04274+2420	173.664	-16.195	3331	-0.03	1.13		-2.03		<0.9	2T	2		FX Tau	2,10
04296+2546	172.887	-14.869	3331	0.26	0.04		-1.36		<0.4	2T	2		UZ Tau E & W	2,10
04300+2403	174.295	-15.918	3331	0.24	0.88		-1.72		<1.0	2T			GH Tau & V807 Tau	2
04306+2514	173.446	-15.056	3331	0.17	0.20		-1.55		<0.3	2T	2		DL Tau, IR Mult.	2,10,33
04308+2244	175.463	-16.637	3331	0.44	0.06		-1.37		<0.5	2T	2		CI Tau	2,10
04315+2232	175.723	-16.647	1131	0.37	1.20		-1.97			1				
04318+2422	174.321	-15.395	3331	0.46	0.96		-1.68		<2.0	2T	2		AA Tau	2,10
04324+2408	174.587	-15.449	1331	0.18	1.15		-1.93			2	2		DN Tau	2,10
04385+2550	174.169	-13.294	3331	0.72	0.44		-1.24		<1.2	2T:	1		Haro 6-33	2,8
<ORION-A>														
05259-0322	206.232	-19.961	1123	0.45	0.77 25	0.12	-0.80 -0.12	0.07	>1.4 -0.83	2				
05261-0418	207.136	-20.353	1132	0.54	0.98 22	0.12	-0.70 0.15	0.07	>2.6 -0.21	3				
05262-0457	207.775	-20.619	1123	0.43	0.91 23	0.07	-0.81 -0.01	0.04	>1.8 -0.49	3				
05275-0500	207.973	-20.365	1123	0.46	1.30 19	0.16	-0.78 0.37	0.08	>4.3 0.51	1				
05279-0227	205.627	-19.088	1123	0.76	0.88 24	0.13	-0.49 0.28	0.06	>3.5 -0.25	1				
05283-0412	207.332	-19.809	1332	1.26	0.66 27	0.13	0.09 0.69	0.05	>4.2 -0.22	1				
05289-0430	207.679	-19.810	3332	0.96	0.32 35	0.12	0.29 0.69	0.05	1.6 -0.87	2E				4B
05295-0548	208.982	-20.282	1132	1.17	0.66 27	0.10	-0.07 0.53	0.04	>6.0 -0.38	3				

Table 2. (Continued)

IRAS NAME (1)	l (2)	b (3)	FQ (4)	60-12 (5)	100-60 Td (6)	Unc. (7)	logL60 logLf (8)	Unc. (9)	Lf/Lm logMenv (10)	OC (11)	SED (12)	Activity (13)	Other Name, Comments (14)	References (15)
05300-0453	208.168	-19.762	1123	1.13	0.74 26	0.16	-0.11 0.55	0.10	>6.5 -0.22	1				
05302-0537	208.899	-20.050	3332	1.08	0.17 39	0.17	1.14 1.49	0.06	1.7 -0.39	2E		O	Ori A-west	4B,13
05304-0435	207.952	-19.518	1323	1.82	-0.04 49	0.15	0.94 1.24	0.06	>5.3 -1.12	2V:				1
05305-0508	208.479	-19.748	3133	1.37	0.48 30	0.13	0.42 0.91	0.07	>7.5 -0.34	1				
05306-0520	208.671	-19.830	2123	0.99	0.68 27	0.17	-0.03 0.59	0.08	>3.8 -0.29	1				
05311-0631	209.855	-20.266	3332	0.70	0.52 30	0.07	0.14 0.64	0.03	1.2 -0.52	3			HH83 IRS, KMS 12	
05319-0551	209.311	-19.777	2322	1.67	0.46 31	0.14	1.56 2.03	0.08	13.3 0.75	1				
05319-0542	209.178	-19.703	3223	1.54	0.28 36	0.13	0.95 1.33	0.08	7.0 -0.31	1				
05322-0443	208.288	-19.197	3123	1.30	0.57 29	0.24	0.78 1.32	0.07	>6.8 0.25	2V:				1
05324-0319	207.002	-18.506	1223	1.01	0.73 26	0.12	-0.23 0.42	0.07	>4.8 -0.36	3				
05327-0457	208.572	-19.183	3323	2.00	0.33 34	0.13	2.66 3.07	0.06	20.8 1.53	2V:		H2O		1,30
05329-0628	210.033	-19.826	3332	1.67	0.47 31	0.17	0.91 1.38	0.05	4.0 0.13	2V			V801 ORI	1
05334-0337	207.413	-18.412	3123	1.05	0.70 26	0.11	0.09 0.72	0.06	>4.9 -0.12	1				
05335-0645	210.360	-19.835	1333	1.23	0.85 24	0.19	0.37 1.11	0.08	>8.1 0.54	2T			V577 Ori,AV Ori,Mlt.	2
05338-0624	210.064	-19.594	3333	2.67	0.37 33	0.14	1.72 2.15	0.06	13.5 0.69	1		O	L1641-N, *IR Cl.*	13,34,37
05338-0529	209.206	-19.186	3322	1.43	0.58 28	0.19	1.40 1.95	0.09	9.7 0.89	1				
05340-0603	209.751	-19.403	2322	1.32	0.95 23	0.12	0.44 1.27	0.06	11.3 0.86	1				
05341-0351	207.700	-18.380	1332	1.00	0.67 27	0.13	-0.13 0.48	0.05	>4.2 -0.41	1				
05353-0644	210.557	-19.417	3322	0.14	0.87 24	0.28	-0.18 0.58	0.23	0.8 0.04	2AE			HD37357	2
05354-0438	208.599	-18.434	3322	0.94	0.92 23	0.12	-0.09 0.72	0.06	5.7 0.25	1				
05356-0541	209.601	-18.877	2323	1.18	0.81 25	0.13	0.04 0.76	0.05	7.6 0.11	1				
05356-0530	209.435	-18.796	1333	1.01	0.62 28	0.09	-0.13 0.44	0.04	>3.9 -0.54	1				
05357-0650	210.708	-19.385	3333	0.28	0.78 25	0.12	0.10 0.79	0.05	1.0 0.09	2AE			N'SK 81	2
05357-0548	209.719	-18.917	3322	1.16	0.77 25	0.14	0.10 0.78	0.08	6.7 0.07	1				
05358-0907	212.881	-20.372	1133	0.91	0.86 24	0.09	-0.34 0.42	0.05	>4.8 -0.15	1				
05358-0704	210.935	-19.448	3333	0.46	-0.07 51	0.11	1.59 1.89	0.06	0.5 -0.54	2V			V883 Ori, Haro 13A	1
05360-0906	212.901	-20.324	1233	0.90	0.77 25	0.12	-0.34 0.34	0.04	>4.0 -0.37	1				

Table 2. (Continued)

IRAS NAME (1)	l (2)	b (3)	FQ (4)	60-12 (5)	100-60 Td (6)	Unc. (7)	logL60 logLf (8)	Unc. (9)	Lf/Lm logMenv (10)	OC (11)	SED (12)	Activity (13)	Other Name, Comments (14)	References (15)
05365-0735	211.502	-19.531	1223	1.12	0.63 27	0.10	-0.09 0.49	0.04	>5.2 -0.47	1				
05366-0902	212.903	-20.140	1133	0.73	0.84 24	0.11	-0.52 0.22	0.06	>3.0 -0.38	1				
05367-0327	207.654	-17.602	1123	1.07	0.73 26	0.13	-0.18 0.47	0.06	>5.4 -0.31	1				
05369-0728	211.440	-19.395	3332	1.89	0.31 35	0.15	1.24 1.63	0.07	11.3 0.06	2E		O	Haro 4-255	2,13
05370-0513	209.340	-18.350	1123	0.87	0.81 25	0.10	-0.37 0.34	0.04	>4.0 -0.30	1				
05375-0924	213.355	-20.119	1133	0.47	1.11 21	0.09	-0.77 0.20	0.04	>2.9 0.05	1				
05375-0731	211.567	-19.294	1333	2.83	0.23 37	0.16	1.60 1.97	0.06	>16.7 0.22	1		O,H2O	L1641-S3	13,16
05378-0750	211.894	-19.351	3332	1.07	0.03 45	0.13	0.43 0.75	0.06	1.5 -1.45	1				
05379-0758	212.028	-19.395	3332	0.66	0.50 30	0.09	0.09 0.58	0.04	1.2 -0.62	1				
05380-0930	213.513	-20.045	1132	0.71	0.83 24	0.09	-0.50 0.23	0.04	>2.5 -0.38	1				
05380-0728	211.581	-19.155	3332	0.79	0.09 43	0.12	1.67 1.99	0.06	1.0 -0.06	2E		N,O	L1641-S, R50	2,13,31
05384-0808	212.246	-19.365	1332	1.61	0.39 33	0.18	0.61 1.05	0.07	>9.7 -0.37	1		O	L1641-S4	13
05386-0426	208.796	-17.631	1123	0.77	0.85 24	0.11	-0.48 0.27	0.05	>3.4 -0.31	1				
05387-0924	213.495	-19.859	3332	1.35	0.18 39	0.10	0.70 1.05	0.04	3.5 -0.81	1		O:		25
05389-0756	212.128	-19.151	1333	1.72	0.32 35	0.09	0.55 0.95	0.05	>3.9 -0.61	1				
05391-0537	209.949	-18.080	3122	1.14	0.59 28	0.16	0.04 0.60	0.07	>4.9 -0.44	1				
05394-0445	209.176	-17.614	3232	1.05	0.68 27	0.09	0.01 0.62	0.03	>4.6 -0.25	1				
05398-0443	209.197	-17.518	1132	1.18	0.68 27	0.21	-0.05 0.56	0.05	6.3 -0.31	1				
05400-0800	212.303	-18.950	2333	0.81	0.75 25	0.10	-0.40 0.26	0.05	2.3 -0.48	2E				4C
05403-0818	212.635	-19.001	3332	1.16	0.08 43	0.10	0.54 0.86	0.05	1.9 -1.22	1		O	L1641-S2	13
05403-0606	210.559	-18.026	1323	1.09	0.81 25	0.11	-0.14 0.57	0.05	>6.5 -0.07	1				
05404-0948	214.073	-19.652	3332	1.15	0.38 33	0.11	1.23 1.67	0.05	3.9 0.22	2				
05409-0623	210.891	-18.023	1123	1.13	0.72 26	0.22	-0.11 0.53	0.07	>6.1 -0.27	1				
05469-0953	214.893	-18.230	1132	0.24	1.20 20	0.16	-0.98 0.07	0.09	>1.9 0.06	3				
05263-0236	205.574	-19.508	1131	0.72	0.76		-0.52			1				
05273-0211	205.315	-19.094	1321	0.86	0.89		-0.37			3				
05281-0259	206.147	-19.297	1131	0.57	1.25		-0.68			1				
05282-0334	206.728	-19.536	1131	0.51	1.31		-0.73			1				
05286-0213	205.506	-18.825	1131	0.56	1.13		-0.48			3				
05287-0543	208.810	-20.431	1131	0.87	1.00		-0.37			1				

Table 2. (Continued)

IRAS NAME (1)	l (2)	b (3)	FQ (4)	60-12 (5)	100-60 Td (6)	Unc. (7)	logL60 logLf (8)	Unc. (9)	Lf/Lm logMenv (10)	OC (11)	SED (12)	Activity (13)	Other Name, Comments (14)	References (15)
05290-0249	206.114	-19.018	1131	0.72	1.24		-0.52			1				
05294-0535	208.768	-20.195	3221	0.66	1.40		-0.41		<8.5	1				
05299-0302	206.425	-18.915	1231	1.19	0.96		-0.06			1				
05299-0250	206.240	-18.814	1321	1.02	1.15		-0.16			1				
05302-0522	208.657	-19.929	1231	0.76	1.07		-0.10			2V:				1
05311-0620	209.678	-20.180	3321	0.79	0.83		-0.30		<2.8	2V				1
05311-0505	208.507	-19.603	1131	1.13	0.71		0.21			3				
05311-0456	208.354	-19.543	1131	0.62	1.25		-0.29			1				
05313-0336	207.135	-18.864	1331	1.14	0.90		-0.07			3				
05314-0546	209.182	-19.840	2231	1.34	0.69		1.27		<8.6	1				
05318-0311	206.814	-18.561	1131	0.57	1.59		-0.55			1				
05320-0434	208.132	-19.159	3121	0.63	1.22		0.19			1				
05320-0431	208.065	-19.151	1131	1.30	0.57		0.23			1				
05325-0612	209.725	-19.808	2331	0.90	1.18		-0.08		<8.5	1				
05327-0446	208.386	-19.109	3121	2.13	0.09		1.82			2V:				1
05332-0437	208.305	-18.932	3231	1.18	-0.06		0.81		<3.1	2V:				1
05332-0431	208.221	-18.879	3131	0.79	0.43		0.24			1				
05333-0543	209.362	-19.391	3321	1.33	-0.80		1.61		<5.8	2V				1
05334-0611	209.817	-19.603	3331	0.49	0.87		0.21		<1.5	2V				1
05338-0647	210.433	-19.770	1131	2.21	0.33		1.29			1		H20	HH1, KMS32	18
05340-0431	208.329	-18.693	3321	0.99	1.33		-0.04		<13.1	1				
05341-0742	211.346	-20.119	1131	1.01	0.69		-0.18			1				
05341-0610	209.879	-19.428	3331	0.86	1.06		-0.07		<5.9	1				
05342-0639	210.356	-19.631	3321	1.13	0.52		0.61		<4.6	1		O		23
05344-0623	210.124	-19.455	1131	0.43	2.57		-0.41			2V				1
05345-0525	209.222	-18.989	2321	1.33	0.64		0.38		<7.6	2V				1
05347-0528	209.305	-18.977	3321	1.21	0.71		0.49		<6.5	1				
05347-0431	208.406	-18.537	1131	1.17	1.05		0.26			3				
05349-0632	210.318	-19.417	2321	0.71	1.30		-0.33		<7.0	1				
05352-0549	209.683	-19.021	1131	1.05	0.79		-0.09			1				
05352-0444	208.658	-18.543	3221	0.70	1.17		-0.26		<5.7	1				
05353-0625	210.267	-19.277	1231	0.63	1.52		-0.43			1				
05355-0658	210.800	-19.489	1331	1.03	1.22		-0.10			2V				1
05356-0610	210.067	-19.096	1231	0.94	1.02		-0.25			1				
05357-0710	211.009	-19.536	2331	0.89	1.62		-0.18		<17.3	1			HH 43 IRS1, Haro 14A	
05359-0515	209.242	-18.613	3321	1.12	0.72		0.66		<5.8	1				
05362-0626	210.389	-19.085	1131	0.89	1.30		-0.17			1				
05362-0523	209.403	-18.612	1131	0.64	1.34		-0.56			1				
05363-0714	211.149	-19.425	3331	-0.13	1.53		-0.35		<1.9	2T			Haro 4-249	2
05363-0702	210.967	-19.336	3331	1.63	0.39		0.78		<4.5	1		O, H2O:	L1641-Center, IR Cl.	13,16,34
05364-0722	211.293	-19.466	3331	0.68	0.88		-0.07		<2.7	2T			Haro 4-254	2
05365-0718	211.240	-19.404	3331	1.09	0.24		0.41		<1.7	2T			V599 Ori	2
05367-0712	211.161	-19.326	1331	1.21	0.37		0.32			1				
05369-0623	210.426	-18.913	3331	1.03	0.90		0.08		<6.4	1				
05371-0353	208.104	-17.712	3231	1.06	0.93		-0.12		<7.6	1				
05371-0338	207.879	-17.598	2321	1.49	0.66		0.57		<11.7	1				
05371-0326	207.682	-17.526	1131	0.90	1.10		-0.27			1				
05376-0547	209.935	-18.480	1331	0.98	1.10		-0.23			1				
05378-0943	213.696	-20.192	3331	-0.03	1.35		-0.66		<1.4	2AE			V350 Ori	2
05379-0815	212.306	-19.525	3331	0.69	0.57		-0.20		<1.5	2				
05380-0744	211.825	-19.279	1331	0.64	1.55		-0.52			1				
05380-0738	211.745	-19.218	1331	0.68	1.54		-0.51			1				
05380-0543	209.924	-18.355	1131	1.06	0.90		-0.15			1				
05382-0855	212.971	-19.747	1131	0.70	0.85		-0.54			1				
05382-0802	212.126	-19.358	1331	0.87	1.22		-0.32			1				

Table 2. (Continued)

IRAS NAME (1)	l (2)	b (3)	FQ (4)	60-12 (5)	100-60 Td (6)	Unc. (7)	logL60 logLf (8)	Unc. (9)	Lf/Lm logMenv (10)	OC (11)	SED (12)	Activity (13)	Other Name, Comments (14)	References (15)
05385-0907	213.197	-19.779	3331	0.28	0.55		-0.30		<0.6	1				
05386-0615	210.502	-18.464	1131	0.82	1.01		-0.40			1				
05388-0858	213.094	-19.646	1331	1.37	0.23		0.15			1				
05389-0752	212.049	-19.131	1321	0.44	1.72		-0.76			1				
05390-0844	212.897	-19.478	1331	1.05	1.00		-0.06			1				
05391-0836	212.788	-19.403	3331	0.99	0.88		0.08		<4.0	1				
05391-0805	212.275	-19.187	3331	0.91	0.52		0.18		<2.0	1				
05392-0809	212.365	-19.190	3321	0.43	1.17		-0.59		<1.9	1				
05393-0822	212.589	-19.260	3331	0.11	1.82		-0.86		<6.4	1				
05394-0802	212.278	-19.096	1331	1.02	0.96		0.04			2	V			1
05395-0632	210.870	-18.400	1321	1.12	0.94		-0.08			1				
05397-0701	211.355	-18.576	1131	0.58	1.53		-0.61			1				
05399-1001	214.223	-19.849	3331	0.88	0.40		0.47		<1.7	1				
05401-1002	214.269	-19.806	3331	0.65	0.43		0.44		<1.1	2	E			4C
05401-0834	212.855	-19.171	1131	0.33	1.62		-0.86			1				
05404-0839	212.981	-19.141	3331	0.46	1.07		-0.32		<2.4	2	E			4C
05405-0952	214.147	-19.639	2321	0.26	1.40		-0.68		<2.7	1				
05405-0834	212.901	-19.083	1321	0.60	1.46		-0.61			2				
05405-0647	211.220	-18.296	1131	0.59	1.49		-0.63			1				
05406-0956	214.224	-19.658	1231	0.67	1.30		-0.56			3				
05407-0845	213.107	-19.128	1331	1.04	0.73		-0.14			1				
05407-0830	212.874	-19.009	1331	0.28	1.42		-0.74			1				
05407-0522	209.918	-17.608	1321	1.42	0.74		0.28			1				
05410-0523	209.967	-17.550	3321	0.79	1.19		-0.20		<7.0	3				
<ORION-B>														
05369-0037	205.060	-16.239	1132	0.64	1.04 22	0.43	-0.61 0.30	0.07	>3.6 0.03	1				
05375-0040	205.176	-16.124	3332	0.80	0.76 25	0.13	0.07 0.75	0.05	2.6 0.01	2	V:			1
05381-0139	206.151	-16.451	1233	1.35	0.79 25	0.16	0.40 1.10	0.07	>9.9 0.42	1				
05385-0247	207.260	-16.893	1223	1.33	0.47 31	0.10	0.46 0.94	0.05	>5.9 -0.32	1				
05385-0212	206.712	-16.636	3223	1.16	0.74 26	0.18	0.83 1.50	0.10	6.8 0.72	1				
05391-0217	206.855	-16.542	3333	1.88	0.27 36	0.08	2.53 2.92	0.03	10.1 1.25	2	VN	O:	NGC 2023,IR Cl.	1,25,35
05392-0249	207.366	-16.748	3322	0.93	0.62 28	0.16	0.21 0.78	0.06	3.2 -0.20	1				
05393-0156	206.562	-16.340	3323	1.42	0.65 27	4.40	3.29 3.88	0.06	2.4 2.96	1		O,H2O	NGC2024/Ori-B,IR Cl.	13,17,35
05394-0253	207.447	-16.759	3333	1.17	0.34 34	0.13	0.53 0.94	0.07	3.8 -0.58	1		O:		25
05398-0304	207.671	-16.745	3333	1.09	0.66 27	0.13	0.14 0.74	0.07	4.8 -0.17	1				
05399-0121	206.098	-15.925	1333	1.94	0.29 35	0.10	0.77 1.16	0.05	>10.8 -0.46	1		O:		25
05405-0117	206.113	-15.768	3332	0.93	0.73 26	0.16	-0.05 0.60	0.06	2.6 -0.18	1				
05407-0212	206.981	-16.151	1123	1.04	0.90 23	0.13	-0.20 0.58	0.05	>7.0 0.09	1				
05413-0104	206.005	-15.482	1233	1.87	0.53 29	0.09	0.64 1.15	0.04	>24.5 0.01	1		O:,H2O	IR Mult.	16,33,25

Table 2. (Continued)

IRAS NAME (1)	l (2)	b (3)	FQ (4)	60-12 (5)	100-60 Td (6)	Unc. (7)	logL60 logLf (8)	Unc. (9)	Lf/Lm logMenv (10)	OC (11)	SED (12)	Activity (13)	Other Name, Comments (14)	References (15)
05427-0116	206.371	-15.270	2333	0.59	1.02 22	0.09	-0.60 0.29	0.05	2.7 -0.01	1				
05429-0236	207.622	-15.833	1223	0.88	0.86 24	0.12	-0.33 0.42	0.06	>4.0 -0.14	1				
05435-0015	205.535	-14.613	3322	1.02	0.51 30	0.26	0.72 1.22	0.17	2.7 0.04	1		O	HH26 IR	13
05437-0001	205.349	-14.454	3332	1.44	0.34 34	0.12	1.77 2.18	0.06	5.6 0.66	3		O,H2O	NGC2068 H2O	13,27
05445-0054	206.254	-14.693	1123	0.32	1.44 18	0.09	-0.90 0.38	0.05	>4.1 0.74	1				
05447+0105	204.475	-13.696	1332	0.74	0.67 27	0.11	-0.38 0.22	0.06	>2.3 -0.66	1				
05450+0019	205.194	-14.012	3332	1.78	0.29 35	0.10	1.11 1.50	0.04	4.9 -0.12	1		O:		25
05451+0037	204.929	-13.838	3322	0.87	0.15 40	0.13	0.85 1.19	0.05	1.2 -0.73	1		O	NGC2071-N	13
05453+0016	205.272	-13.955	1133	0.77	1.06 21	0.11	-0.47 0.46	0.05	>5.2 0.22	1				
05457-0135	207.025	-14.745	1123	0.82	0.96 23	0.09	-0.43 0.41	0.06	>4.7 0.01	1				
05461-0118	206.808	-14.537	1132	0.90	0.74 26	0.16	-0.34 0.32	0.08	>3.8 -0.45	1				
05462-0124	206.916	-14.563	1233	1.18	0.56 29	0.11	-0.06 0.47	0.04	>5.5 -0.62	3		O:		25
05464+0106	204.655	-13.317	3332	0.48	0.64 27	0.15	-0.21 0.38	0.07	1.1 -0.57	2T				3
05478-0046	206.532	-13.913	1133	0.87	0.83 24	0.09	-0.37 0.36	0.03	>4.2 -0.25	1				
05482-0138	207.368	-14.231	1132	0.55	0.82 24	0.09	-0.69 0.03	0.04	>2.0 -0.60	3				
05484-0017	206.163	-13.549	1132	0.76	0.55 29	0.12	-0.46 0.07	0.04	>2.0 -1.04	1				
05487+0113	204.843	-12.751	1123	0.57	0.88 24	0.13	-0.64 0.13	0.06	>2.2 -0.40	1				
05490-0027	206.385	-13.485	1133	0.68	0.65 27	0.10	-0.56 0.03	0.05	>1.9 -0.89	3				
05494+0121	204.800	-12.555	1123	0.92	0.71 26	0.13	-0.32 0.32	0.04	>3.7 -0.50	1				
05368-0126	205.791	-16.646	1331	1.02	0.89		0.01			3				
05371-0117	205.707	-16.500	1131	1.12	0.41		-0.13			1				
05374-0134	205.998	-16.572	3231	1.06	0.88		0.07		<6.9	3				
05379-0142	206.176	-16.528	1231	1.28	0.82		0.37			1				
05382-0209	206.630	-16.677	3121	1.26	1.01		0.55			1				
05382-0114	205.793	-16.239	1131	1.12	0.99		0.05			1				
05384-0309	207.571	-17.093	1131	0.91	0.99		-0.28			1				
05385-0136	206.154	-16.346	1231	1.14	0.65		0.35			1				
05386-0229	206.991	-16.736	3321	1.26	0.83		0.69		<9.0	1				
05386-0156	206.481	-16.490	3121	2.08	0.35		2.10			1				
05387-0234	207.082	-16.747	3331	1.18	0.70		0.46		<6.2	2V				1
05391-0152	206.479	-16.349	3231	1.68	1.05		2.86		<26.1	1				
05392-0145	206.389	-16.264	3331	1.38	-0.94		1.76		<6.3	1				
05393-0126	206.104	-16.093	1131	0.85	1.24		-0.32			1				
05394-0303	207.606	-16.828	3321	1.07	1.21		0.35		<13.7	1				
05394-0151	206.505	-16.268	2321	1.52	1.97		1.85		<156.0	3N				

Table 2. (Continued)

IRAS NAME (1)	l (2)	b (3)	FQ (4)	60-12 (5)	100-60 Td (6)	Unc. (7)	logL60 logLf (8)	Unc. (9)	Lf/Lm logMenv (10)	OC (11)	SED (12)	Activity (13)	Other Name,Comments (14)	References (15)
05395-0259	207.558	-16.779	3331	0.98	0.59		0.30		<3.5	1				
05398-0346	208.330	-17.065	1131	0.71	1.28		-0.45			3				
05399-0251	207.477	-16.618	3331	1.02	0.71		0.06		<4.5	1				
05399-0247	207.423	-16.584	1131	0.81	1.47		-0.43			1				
05400-0158	206.668	-16.195	3221	0.97	0.38		0.67		<2.6	1				
05402-0326	208.061	-16.819	1131	1.05	0.84		0.02			1				
05403-0131	206.294	-15.916	1131	0.68	1.49		-0.36			1				
05404-0158	206.726	-16.093	3121	0.90	0.87		0.12			1				
05407-0139	206.484	-15.877	1131	1.07	1.24		-0.06			1				
05408-0339	208.332	-16.795	3221	0.52	1.18		-0.15		<3.8	1				
05408-0131	206.371	-15.793	1131	0.52	1.52		-0.38			1				
05410-0203	206.887	-16.004	1131	0.45	1.48		-0.55			1				
05415-0206	206.988	-15.924	1131	0.43	1.51		-0.70			1				
05417-0120	206.317	-15.507	1231	0.70	1.37		-0.35			2				
05421-0145	206.734	-15.615	1131	0.57	1.70		-0.67			1				
05425-0352	208.736	-16.513	1131	0.76	0.86		-0.45			1				
05428-0317	208.229	-16.193	1321	0.87	1.15		-0.35			1				
05432-0310	208.182	-16.035	2231	0.90	0.99		-0.27		<5.5	1				
05433-0231	207.597	-15.714	1231	0.54	1.72		-0.70			1				
05435-0238	207.707	-15.733	1131	0.56	1.56		-0.67			3				
05435-0014	205.531	-14.601	1131	1.76	-0.01		0.89			1				
05435-0011	205.476	-14.568	3331	1.09	0.06		0.83		<1.6	3N		O,H2O	HH24	13,19
05445+0020	205.109	-14.110	3331	1.22	0.15		2.22		<2.0	1	1	O,H2O,HII	NGC2071, IR Cl.	13,16,21,35
05446-0242	207.918	-15.513	1131	0.42	1.72		-0.81			2E				4A
05449+0050	204.722	-13.775	1131	0.34	1.54		-0.86			1				
05450-0121	206.722	-14.792	3231	0.96	1.10		-0.28		<8.5	1				
05453-0218	207.636	-15.178	3331	0.47	1.41		-0.47		<5.7	2V:				1
05454+0034	205.011	-13.800	1331	1.37	0.50		0.20			1				
05459-0123	206.867	-14.608	1131	0.87	0.84		-0.35			1				
05469-0127	207.039	-14.424	1131	0.83	0.88		-0.38			1				
05469-0121	206.952	-14.384	1131	0.50	1.28		-0.75			3				
05469+0059	204.821	-13.258	1131	0.54	1.09		-0.70			1				
05474-0103	206.749	-14.120	1131	0.73	0.72		-0.52			1				
05476-0122	207.055	-14.233	1131	0.43	0.93		-0.77			1				
05493+0051	205.246	-12.801	1131	0.45	1.53		-0.74			3				
05497+0102	205.118	-12.638	1331	0.46	1.49		-0.73			2				
05498+0043	205.419	-12.768	1131	0.81	1.21		-0.40			1				
05506+0031	205.703	-12.672	1131	0.86	1.00		-0.39			3				
<VELA>														
08343-4052	260.332	-0.196	1123	0.64	0.87 24	0.12	-0.32 0.44	0.06	>2.6 -0.10	3				
08355-4027	260.151	0.248	3333	1.04	0.16 40	0.10	0.55 0.89	0.04	0.7 -1.01	1				
08363-4126	261.029	-0.235	1132	0.76	0.87 24	0.11	-0.19 0.57	0.05	>3.5 0.03	1				
08373-4059	260.781	0.194	3333	1.56	0.22 38	0.09	1.03 1.39	0.04	4.0 -0.38	1		O:	DC260.8+0.2	14
08373-4037	260.481	0.411	1123	1.32	0.67 27	0.12	0.37 0.97	0.04	>8.8 0.09	1				
08375-4109	260.926	0.115	3332	1.36	0.19 39	0.09	1.95 2.30	0.05	2.3 0.47	1	1		VMR IRS 13, IR Mult.	5
08375-4046	260.632	0.343	2233	0.90	0.68 27	0.08	-0.02 0.59	0.03	3.4 -0.28	1				

Table 2. (Continued)

IRAS NAME (1)	l (2)	b (3)	FQ (4)	60-12 (5)	100-60 Td (6)	Unc. (7)	logL60 logLf (8)	Unc. (9)	Lf/Lm logMenv (10)	OC (11)	SED (12)	Activity (13)	Other Name, Comments (14)	References (15)
08378-4144	261.416	-0.200	2133	1.35	0.44 31	0.06	0.33 0.80	0.03	>6.6 -0.53	3				
08380-4100	260.868	0.275	1322	1.39	0.67 27	0.11	0.50 1.11	0.05	>9.5 0.22	1				
08381-4101	260.885	0.284	1322	1.13	0.99 22	0.25	0.21 1.07	0.18	>9.5 0.73	1				
08393-4041	260.775	0.678	3333	1.68	0.41 32	0.18	1.51 1.96	0.08	9.4 0.58	2	1	O:	VMR IRS 63	9,14
08398-4125	261.409	0.297	1322	0.90	0.44 31	0.16	0.22 0.68	0.08	>2.0 -0.64	3				
08398-4104	261.129	0.512	3322	0.75	0.76 25	0.11	0.10 0.78	0.05	2.7 0.04	1				
08400-4007	260.404	1.125	1123	0.93	0.70 26	0.07	-0.01 0.61	0.03	>3.7 -0.22	3				
08404-4054	261.071	0.702	1132	0.60	0.87 24	0.09	-0.23 0.53	0.05	>1.9 -0.01	1				
08404-4033	260.796	0.918	3333	0.84	0.28 36	0.12	1.25 1.64	0.07	1.5 -0.01	2EN	1	O:	ESO 313-N*10	2,5,14
08408-3931	260.035	1.614	1133	0.60	0.85 24	0.11	-0.34 0.41	0.05	>2.3 -0.17	3				
08412-4041	260.989	0.947	1223	0.90	1.20 20	0.19	-0.03 1.03	0.13	>9.1 1.01	3				
08414-4110	261.404	0.682	3232	0.91	0.90 23	0.18	0.30 1.08	0.05	5.2 0.59	1				
08415-3934	260.156	1.682	1123	0.81	0.87 24	0.13	-0.14 0.62	0.07	>3.9 0.08	3				
08416-4222	262.364	-0.030	1123	0.80	1.09 21	0.15	-0.15 0.81	0.08	>5.8 0.62	3				
08416-4058	261.274	0.840	3122	1.44	0.76 25	0.10	1.05 1.73	0.04	>10.4 0.99	1				
08417-4040	261.045	1.034	1322	1.17	0.91 23	0.17	0.41 1.20	0.07	>6.1 0.73	2				
08421-4306	262.990	-0.424	3323	0.98	0.79 25	0.11	0.31 1.01	0.05	4.8 0.33	1				
08421-3944	260.359	1.679	2123	0.67	0.93 23	0.12	-0.36 0.45	0.06	>3.0 0.01	2				
08427-4124	261.734	0.724	3122	0.94	1.15 20	0.13	0.46 1.47	0.07	>8.8 1.38	1				
08431-4220	262.507	0.206	1323	0.85	0.83 24	0.09	-0.08 0.65	0.04	>3.9 0.04	3				
08433-4125	261.820	0.812	2322	1.26	1.00 22	0.12	0.69 1.57	0.05	14.4 1.23	1				
08435-4105	261.580	1.055	3222	1.25	0.66 27	0.19	1.38 1.98	0.09	7.0 1.07	1				
08438-4201	262.337	0.495	1333	0.94	0.65 27	0.09	0.05 0.64	0.03	>2.4 -0.28	3				
08439-4147	262.169	0.666	1123	0.83	1.01 22	0.10	-0.11 0.77	0.04	>5.2 0.46	3				
08442-4328	263.524	-0.347	1322	1.49	0.43 32	0.11	1.31 1.77	0.05	>8.5 0.43	3		O:	VHE21A,BBW182	14
08448-4343	263.776	-0.428	3333	1.55	0.48 30	0.13	2.21 2.70	0.06	3.9 1.45	1	1	O:	VMR IRS 17, IR Neb.	5,14
08448-4233	262.879	0.310	1332	1.17	0.79 25	0.13	0.24 0.94	0.06	>7.5 0.26	1				

Table 2. (Continued)

IRAS NAME (1)	l (2)	b (3)	FQ (4)	60-12 (5)	100-60 Td (6)	Unc. (7)	logL60 logLf (8)	Unc. (9)	Lf/Lm logMenv (10)	OC (11)	SED (12)	Activity (13)	Other Name, Comments (14)	References (15)
08455-4105	261.808	1.337	1223	0.90	0.79 25	0.11	-0.05 0.64	0.05	>4.1 -0.03	1				
08456-4327	263.655	-0.142	3322	0.32	0.87 24	0.13	0.19 0.95	0.06	1.3 0.41	1				
08457-4229	262.934	0.480	1123	1.09	0.72 26	0.25	0.15 0.79	0.19	>5.5 -0.01	1				
08457-4124	262.094	1.169	1132	1.24	0.91 23	0.13	0.28 1.07	0.06	>11.0 0.60	1				
08458-4332	263.751	-0.162	3323	1.21	0.46 31	0.12	0.95 1.42	0.05	4.1 0.14	1				
08459-4338	263.850	-0.216	1232	1.34	0.78 25	0.13	0.48 1.17	0.06	>9.6 0.47	1				
08460-4223	262.888	0.581	3222	1.42	0.58 28	0.09	0.76 1.30	0.04	9.7 0.25	1				
08466-4224	262.977	0.662	1333	1.97	0.43 32	0.16	1.50 1.96	0.07	>11.9 0.62	1		0:		14
08466-4119	262.133	1.352	3323	1.19	0.79 25	0.09	0.33 1.03	0.05	7.5 0.35	1				
08470-4321	263.741	0.115	3333	0.86	0.08 43	0.16	2.22 2.54	0.06	1.2 0.46	3	1	0:	VMR IRS 19	5,14
08470-4243	263.249	0.515	3333	1.79	0.27 36	0.07	2.68 3.06	0.03	7.3 1.40	2	1	0:	VMR IRS 18	5,14
08470-4208	262.807	0.897	2322	0.91	0.87 24	0.12	0.05 0.81	0.06	4.7 0.27	1				
08471-4346	264.080	-0.143	1123	1.26	0.84 24	0.12	0.39 1.13	0.08	>9.2 0.53	3				
08476-4306	263.619	0.366	3332	1.55	0.36 33	0.12	2.04 2.46	0.06	4.2 0.98	3	1	0:	VMR IRS 20	5,14
08476-4247	263.387	0.565	1322	1.44	0.48 30	0.11	0.54 1.03	0.06	>7.2 -0.22	3				
08476-4212	262.929	0.937	3322	1.02	0.69 26	0.11	0.45 1.07	0.05	4.5 0.22	1				
08477-4359	264.322	-0.184	3333	1.53	0.26 36	0.14	2.20 2.58	0.06	6.4 0.89	1	1		VMR IRS 21	5
08479-4058	262.022	1.762	1322	1.23	0.85 24	0.19	0.33 1.07	0.08	>7.9 0.50	3				
08485-4419	264.669	-0.284	3332	1.74	0.07 44	0.12	2.62 2.94	0.05	3.2 0.84	1	1	0:	VMR IRS 22	5,14
08491-4310	263.851	0.535	2322	1.20	0.71 26	0.09	0.56 1.19	0.04	7.0 0.38	3				
08500-4414	264.773	-0.020	1123	0.82	1.00 22	0.24	-0.10 0.77	0.17	>4.9 0.44	3				
08500-4254	263.743	0.824	3333	1.16	0.21 38	0.09	1.11 1.47	0.04	2.8 -0.32	2E	1		VMR IRS 71	4,9
08500-4237	263.531	1.011	3323	1.38	0.66 27	0.11	1.33 1.93	0.04	10.0 1.02	1				
08500-4143	262.843	1.581	1123	0.76	0.73 26	0.13	-0.12 0.54	0.08	>1.6 -0.25	1				
08504-4241	263.637	1.027	2232	1.32	0.79 25	0.16	0.43 1.12	0.07	10.9 0.45	1				
08509-4325	264.251	0.613	3322	1.30	0.46 31	0.12	1.17 1.64	0.06	5.8 0.36	3				
08511-4229	263.564	1.252	1333	1.14	0.71 26	0.11	0.35 0.98	0.07	>6.1 0.17	3				

Table 2. (Continued)

IRAS NAME (1)	l (2)	b (3)	FQ (4)	60-12 (5)	100-60 Td (6)	Unc. (7)	logL60 logLf (8)	Unc. (9)	Lf/Lm logMenv (10)	OC (11)	SED (12)	Activity (13)	Other Name, Comments (14)	References (15)
08513-4201	263.227	1.571	3333	1.54	0.13 41	0.10	2.35 2.68	0.04	2.5 0.72	3N	1	O:	VMR IRS 26/1,2	5,14
08516-4338	264.510	0.577	1233	1.26	0.59 28	0.11	0.36 0.91	0.05	>5.8 -0.12	3				
08519-4239	263.786	1.244	2133	0.94	0.63 27	0.17	0.18 0.76	0.12	>3.4 -0.20	1				
08520-4412	264.971	0.260	3332	0.55	0.44 31	0.16	1.22 1.68	0.07	1.1 0.36	1				
08525-4206	263.438	1.701	1132	0.86	0.81 25	0.14	-0.07 0.64	0.06	>3.8 -0.00	1				
08527-4357	264.870	0.520	1133	1.09	0.68 27	0.13	0.16 0.78	0.07	>5.0 -0.10	3				
08533-4417	265.188	0.395	1332	1.40	0.74 26	0.41	0.52 1.18	0.06	>7.8 0.41	3				
08534-4231	263.863	1.548	3333	1.14	0.38 33	0.13	0.83 1.26	0.06	3.8 -0.18	3			VMR IRS 73/1,2	9
08546-4254	264.292	1.471	3332	1.63	0.19 39	0.13	2.82 3.17	0.04	4.8 1.34	2AEN		HII,H2O	RCW 34, G264.292	4,20
08551-4344	264.987	0.987	3332	0.76	0.27 36	0.19	0.89 1.27	0.13	1.0 -0.39	1				
08555-4412	265.393	0.746	1123	0.98	0.85 24	0.14	0.05 0.79	0.06	>5.4 0.22	1				
08563-4225	264.143	2.019	3333	1.31	0.23 37	0.15	2.21 2.58	0.07	3.5 0.83	1	1	O:	VMR IRS31/1,2,3	5,14
08565-4318	264.820	1.462	1332	1.31	0.45 31	0.13	0.41 0.88	0.06	>5.4 -0.42	1				
08566-4313	264.779	1.532	3322	1.27	0.41 32	0.22	0.59 1.04	0.08	5.6 -0.34	2AE			Herbst 28	2
08574-4254	264.637	1.851	1233	1.20	0.54 29	0.08	0.26 0.77	0.04	>5.4 -0.35	1				
08576-4334	265.148	1.443	2223	2.07	0.27 36	0.14	3.62 4.00	0.09	11.4 2.34	2AEN		O:,H2O	RCW 36	2,14,20
08576-4314	264.901	1.658	3332	0.93	-0.21 62	0.15	1.30 1.60	0.07	0.9 -1.19	1	1		VMR IRS 33	5
08578-4300	264.759	1.846	1132	1.13	0.61 28	0.09	0.23 0.80	0.04	>3.9 -0.20	1				
08587-4419	265.850	1.093	1233	1.45	0.55 29	0.10	0.55 1.08	0.05	>8.1 -0.03	1		O:		14
08339-4056	260.348	-0.288	3121	0.29	1.47		-0.51			3				
08342-4033	260.080	-0.008	3321	1.15	0.81		0.42		<7.1	1				
08343-4106	260.522	-0.323	1131	0.51	1.56		-0.45			3				
08343-4039	260.161	-0.067	1321	1.03	0.93		0.08			1				
08348-4040	260.246	0.007	1331	0.79	1.16		-0.16			3				
08358-4046	260.440	0.098	1131	0.36	1.83		-0.58			3				
08368-4102	260.753	0.076	1131	0.71	1.42		-0.24			1				
08370-4040	260.492	0.329	1331	0.67	1.45		-0.23			2				
08373-4049	260.653	0.286	3331	0.69	1.22		-0.06		<4.6	1				
08379-4056	260.800	0.309	1131	0.74	1.40		-0.22			3				
08386-4051	260.819	0.459	1131	0.50	1.63		-0.45			3				
08387-4014	260.350	0.852	1131	0.42	1.57		-0.51			3				
08389-4215	261.953	-0.351	1131	0.48	1.69		-0.47			3				
08390-4015	260.406	0.897	1131	0.62	0.96		-0.33			3				
08392-4200	261.803	-0.152	1131	0.65	1.48		-0.29			3				
08393-4110	261.158	0.372	1131	0.69	1.43		-0.22			3				

Table 2. (Continued)

IRAS NAME (1)	l (2)	b (3)	FQ (4)	60-12 (5)	100-60 Td (6)	Unc. (7)	logL60 logLf (8)	Unc. (9)	Lf/Lm logMenv (10)	OC (11)	SED (12)	Activity (13)	Other Name,Comments (14)	References (15)
08394-4225	262.157	-0.386	1331	1.31	0.56		0.43			2				
08397-4039	260.791	0.759	1131	0.70	1.83		-0.01			3				
08398-4018	260.524	0.978	1131	0.81	1.31		-0.14			3				
08406-4242	262.507	-0.384	1131	0.73	1.34		-0.22			3				
08407-4114	261.359	0.536	1131	-0.06	1.71		-0.50			3				
08407-4043	260.967	0.866	1331	1.22	0.86		0.33			1				
08412-4103	261.285	0.724	1231	1.05	0.89		0.14			1				
08415-4028	260.865	1.138	1131	0.63	1.29		-0.26			3				
08420-4132	261.750	0.538	1331	0.92	0.94		0.26			2				
08420-4118	261.579	0.691	1131	1.06	1.01		0.65			3				
08424-4122	261.680	0.704	3221	1.19	1.17		0.56		<15.8	1				
08424-4100	261.381	0.937	3221	1.21	1.53		0.74		<41.5	1				
08425-4119	261.643	0.746	2131	1.02	1.31		0.36			1				
08427-4158	262.181	0.368	1131	1.05	0.83		0.10			3				
08429-4055	261.377	1.051	3321	1.18	0.86		0.93		<8.9	1				
08429-4037	261.150	1.242	1231	0.84	1.40		-0.10			3				
08432-4258	263.005	-0.178	1131	0.73	1.28		-0.22			3				
08432-4046	261.297	1.188	2231	1.22	0.61		0.44		<6.3	3				
08433-4326	263.384	-0.462	3331	0.28	1.00		0.08		<1.5	1				
08437-4059	261.529	1.140	2321	1.15	0.55		0.83		<4.5	1				
08441-4244	262.942	0.099	1131	0.48	1.46		-0.40			3				
08441-4153	262.275	0.624	3331	1.20	0.53		0.40		<3.3	1				
08446-4112	261.793	1.134	3321	0.52	1.32		0.21		<5.0	3				
08448-4057	261.636	1.325	1231	0.59	1.55		-0.26			3				
08449-4137	262.165	0.908	3221	0.64	1.33		-0.25		<6.9	3				
08450-4123	261.993	1.067	2231	1.00	0.99		0.12		<7.6	1				
08461-4314	263.550	0.056	3321	0.91	0.94		0.41		<5.6	1				
08462-4235	263.063	0.495	1131	0.67	1.40		-0.17			3				
08463-4343	263.948	-0.215	1231	1.39	0.78		0.53			3				
08465-4230	263.030	0.586	1231	0.70	2.04		-0.24			3				
08467-4110	262.034	1.462	1321	0.82	1.09		-0.02			3				
08468-4330	263.840	0.002	1321	1.00	1.01		0.15			3				
08471-4228	263.065	0.690	3321	1.37	1.18		0.70		<27.4	3				
08471-4113	262.111	1.482	2331	1.11	0.84		0.25		<7.0	1				
08472-4326	263.839	0.095	3331	0.90	1.72		0.49		<31.0	2				
08476-4109	262.115	1.607	1131	0.67	1.29		-0.27			3				
08478-4120	262.289	1.511	3321	0.68	1.68		0.24		<15.6	1				
08480-4206	262.892	1.052	1131	0.62	1.35		-0.33			3				
08481-4258	263.578	0.526	1321	1.22	0.66		0.56			3				
08485-4414	264.599	-0.246	3321	0.90	0.23		1.00		<1.4	1	1		VMR IRS 76	40
08487-4203	262.945	1.186	1321	1.03	0.78		0.18			3				
08488-4308	263.788	0.508	3221	0.88	0.77		0.70		<3.7	3				
08488-4233	263.347	0.879	2321	1.05	1.08		0.37		<10.0	3				
08493-4339	264.248	0.244	1321	1.01	1.10		0.19			3				
08494-4326	264.092	0.406	1321	1.21	0.54		0.43			3				
08495-4306	263.848	0.619	1131	0.81	1.31		-0.07			3				
08495-4238	263.492	0.925	1331	1.58	1.02		0.95			3				
08496-4320	264.034	0.497	3331	1.13	0.69		0.56		<5.8	3				
08506-4146	262.953	1.638	1131	0.90	0.57		0.13			3				
08506-4134	262.793	1.769	1131	0.38	1.30		-0.30			3				
08507-4256	263.853	0.907	1131	0.89	1.17		-0.06			3				
08508-4404	264.742	0.179	3221	1.47	0.45		0.85		<8.9	3				
08508-4334	264.357	0.512	1131	0.76	1.34		-0.08			3				
08513-4351	264.636	0.393	1131	0.55	1.48		-0.27			3				
08514-4241	263.743	1.157	2331	0.70	1.35		-0.01		<8.0	1				

Table 2. (Continued)

IRAS NAME (1)	l (2)	b (3)	FQ (4)	60-12 (5)	100-60 Td (6)	Unc. (7)	logL60 logLf (8)	Unc. (9)	Lf/Lm logMenv (10)	OC (11)	SED (12)	Activity (13)	Other Name, Comments (14)	References (15)
08514-4141	262.985	1.807	1321	1.08	0.85		0.15			3				
08517-4326	264.352	0.724	1131	1.09	0.91		0.17			3				
08518-4130	262.890	1.979	1331	0.84	1.28		0.08			3				
08520-4359	264.812	0.414	1131	0.89	0.95		0.05			3				
08520-4303	264.099	1.000	3221	1.06	0.84		0.31		<6.4	1				
08520-4231	263.687	1.357	2131	0.77	1.66		-0.23			3				
08521-4258	264.044	1.081	1131	0.54	1.27		0.06			3				
08523-4335	264.540	0.697	1131	0.89	0.92		0.09			3				
08524-4518	265.869	-0.390	1131	0.89	0.58		0.23			3				
08527-4329	264.513	0.834	1131	0.54	1.46		-0.36			3				
08534-4301	264.238	1.221	3331	0.60	1.18		-0.04		<4.0	3				
08539-4432	265.452	0.308	3331	1.04	0.73		0.40		<4.1	1				
08539-4413	265.218	0.516	3321	1.39	0.36		0.75		<3.4	2				
08540-4316	264.500	1.148	1331	1.43	0.44		0.55			3				
08549-4327	264.749	1.148	3321	-0.02	1.69		-0.52		<3.5	3				
08555-4244	264.274	1.707	3331	1.05	0.45		0.66		<2.1	1				
08557-4323	264.803	1.302	1331	1.44	0.64		0.56			1				
08559-4238	264.250	1.817	1321	1.30	1.06		0.42			1				
08568-4232	264.289	2.012	3321	1.04	0.72		0.59		<3.2	1				
08574-4223	264.246	2.198	1321	0.53	1.39		-0.39			1				
08575-4330	265.093	1.473	3321	1.33	1.52		2.29		<51.6	3N	1		VMR IRS 32/1,2	5
08576-4320	264.977	1.594	1331	1.85	0.11		1.09			1				
08580-4344	265.336	1.393	3331	1.13	0.36		1.08		<2.9	1	1			9
08580-4339	265.268	1.444	3321	1.27	0.69		1.02		<8.0	1				
08581-4422	265.813	0.986	1331	0.83	0.37		0.23			1				
08588-4347	265.463	1.455	3321	0.80	0.17		1.26		<1.1	1				
08589-4423	265.928	1.075	2331	0.90	0.49		0.28		<2.1	1				
08592-4359	265.653	1.380	1131	0.90	1.28		0.00			1				
<ρ-Oph.>														
16145-2352	351.957	18.696	1133	0.63	0.98 22	0.09	-1.79 -0.94	0.05	>2.9 -1.30	1				
16177-2326	352.816	18.440	1122	0.90	0.82 24	0.10	-1.36 -0.64	0.06	>4.3 -1.27	1				
16200-2251	353.655	18.444	1133	1.49	0.82 24	0.12	-0.87 -0.15	0.05	>15.0 -0.78	1				
16214-2436	352.509	17.033	1132	1.17	0.78 25	0.13	-1.19 -0.50	0.07	>6.3 -1.20	1				
16228-2411	353.049	17.075	3223	1.39	0.67 27	0.16	0.42 1.02	0.08	10.2 0.14	1			L1686	
16240-2430	352.999	16.652	3332	0.71	0.47 31	0.15	0.50 0.97	0.07	1.4 -0.28	1	1		WL16	12
16243-2311	354.086	17.471	1123	1.11	1.03 22	0.21	-1.24 -0.34	0.13	>10.0 -0.62	1				
16250-2302	354.312	17.463	1133	1.19	0.77 25	0.12	-1.24 -0.55	0.05	>7.2 -1.27	1				
16250-2248	354.486	17.605	1123	0.82	0.94 23	0.12	-1.52 -0.71	0.06	>4.1 -1.13	1				
16253-2429	353.211	16.443	1133	1.05	0.76 25	0.13	-1.36 -0.69	0.05	>5.1 -1.42	1				
16261-2249	354.659	17.396	1133	0.78	0.93 23	0.13	-1.63 -0.82	0.06	>3.8 -1.26	1				
16265-2350	353.906	16.673	1132	0.90	0.86 24	0.11	-1.50 -0.75	0.03	>4.2 -1.31	2				

Table 2. (Continued)

IRAS NAME (1)	l (2)	b (3)	FQ (4)	60-12 (5)	100-60 Td (6)	Unc. (7)	logL60 logLf (8)	Unc. (9)	Lf/Lm logMenv (10)	OC (11)	SED (12)	Activity (13)	Other Name,Comments (14)	References (15)
16266-2301	354.563	17.189	1132	0.67	0.96 23	0.14	-1.75 -0.90	0.05	>3.0 -1.31	1				
16281-2514	353.070	15.464	1132	0.80	0.83 24	0.10	-1.63 -0.89	0.06	>3.3 -1.51	3				
16284-2418	353.852	16.034	3332	0.17	0.88 24	0.13	-1.54 -0.77	0.05	0.9 -1.30	2T:			WSB 71	2
16288-2450	353.501	15.614	3322	1.25	0.27 36	0.14	0.02 0.41	0.06	2.8 -1.26	1		0	L1709	13
16293-2422	353.936	15.840	1333	2.97	0.61 28	0.09	0.60 1.16	0.05	158.0 0.17	1	1	0,H2O	ρ Oph-S, L1687-N	12A,13,19
16293-2358	354.242	16.092	1123	0.56	1.18 20	0.14	-1.83 -0.80	0.07	>3.1 -0.84	1				
16305-2425	354.081	15.598	1123	0.49	1.41 18	0.14	-1.79 -0.52	0.05	>5.8 -0.22	1				
16313-2439	354.028	15.301	1133	0.54	1.19 20	0.08	-1.86 -0.82	0.03	>3.6 -0.84	3				
16335-2419	354.616	15.132	1133	0.35	1.03 22	0.12	-1.97 -1.07	0.05	>1.8 -1.35	2				
16369-2247	356.360	15.520	1133	0.38	1.01 22	0.07	-2.04 -1.16	0.04	>1.7 -1.47	1				
16375-2439	354.949	14.231	1133	0.53	1.10 21	0.08	-1.88 -0.92	0.04	>3.0 -1.09	3				
16384-2206	357.136	15.677	1132	0.44	0.70 26	0.10	-1.91 -1.28	0.03	>1.2 -2.12	1				
16417-2155	357.783	15.212	1132	0.45	1.10 21	0.09	-1.89 -0.93	0.05	>2.2 -1.10	1				
16421-2404	356.099	13.796	1123	0.65	0.94 23	0.14	-1.76 -0.95	0.07	>2.9 -1.37	1				
16426-2129	358.262	15.321	1133	0.25	0.92 23	0.11	-2.14 -1.34	0.04	>1.1 -1.80	1				
16430-2128	358.339	15.243	1123	0.07	1.09 21	0.07	-2.17 -1.22	0.03	>1.1 -1.40	1				
16460-2358	356.764	13.154	1132	0.63	0.86 24	0.10	-1.80 -1.05	0.05	>2.4 -1.61	1				
16149-2338	352.210	18.765	1131	0.96	0.24		-1.42			1				
16153-2327	352.421	18.831	1131	0.53	0.68		-1.76			1				
16156-2358	352.064	18.445	3331	1.13	-0.20		-0.84		<2.0	2				
16161-2419	351.874	18.112	1231	1.27	0.38		-1.04			2				
16164-2435	351.717	17.876	1131	0.74	0.69		-1.41			1				
16173-2422	352.041	17.873	1131	0.82	1.17		-1.48			1				
16184-2452	351.823	17.349	1331	1.65	0.44		-0.73			1				
16194-2500	351.878	17.100	1131	0.92	1.23		-1.44			1				
16194-2410	352.521	17.657	1131	0.81	1.39		-1.54			3				
16196-2443	352.133	17.256	1131	1.14	0.40		-1.05			1				
16197-2358	352.733	17.729	3121	0.63	1.32		-1.51			1				
16201-2410	352.642	17.546	1331	1.28	0.82		-1.06			2				
16202-2427	352.436	17.324	1131	0.53	1.33		-1.60			1				
16203-2332	353.176	17.931	1131	1.18	1.09		-1.17			1				
16214-2345	353.171	17.604	1131	1.26	0.90		-0.97			1				
16219-2514	352.097	16.522	3131	0.67	1.46		-1.63			2				
16219-2344	353.259	17.523	1131	0.84	1.15		-1.31			1				
16234-2436	352.816	16.692	3331	0.97	0.53		-0.89		<2.9	1				
16238-2317	353.935	17.493	1131	0.87	0.97		-1.37			3				
16239-2438	352.874	16.582	3331	0.36	0.68		-0.89		<0.9	2T			SR 24S & SR 24N	2

Table 2. (Continued)

IRAS NAME (1)	l (2)	b (3)	FQ (4)	60-12 (5)	100-60 Td (6)	Unc. (7)	logL60 logLf (8)	Unc. (9)	Lf/Lm logMenv (10)	OC (11)	SED (12)	Activity (13)	Other Name, Comments (14)	References (15)
16241-2412	353.252	16.834	3331	1.13	0.70		-0.29		<2.3	2T			El 30	2
16242-2258	354.247	17.632	1131	1.08	0.98		-1.22			3				
16246-2440	352.973	16.436	1131	1.01	1.09		-1.35			1				
16246-2436	353.014	16.488	3321	0.41	0.85		-1.18		<1.4	1				
16246-2259	354.283	17.556	1131	0.86	1.20		-1.53			3				
16247-2314	354.109	17.374	1131	0.82	1.13		-1.46			1				
16247-2247	354.458	17.666	1131	0.69	1.40		-1.69			1				
16257-2421	353.376	16.467	3231	0.35	1.51		-1.67		<5.3	2T			V853 Oph	2
16262-2317	354.300	17.083	1131	0.04	1.69		-2.16			1				
16269-2454	353.135	15.901	1131	1.49	0.89		-0.89			1				
16275-2251	354.849	17.147	1131	-0.20	1.84		-2.32			3				
16285-2519	353.068	15.359	1131	0.72	1.06		-1.64			3				
16285-2355	354.171	16.267	3331	0.84	0.83		-0.86		<2.9	1			L1709B	
16289-2527	353.012	15.197	1131	0.61	1.53		-1.81			3				
16289-2457	353.411	15.535	3321	0.46	1.61		-1.46		<7.4	1T:			WSB 73 & WSB 74	2
16301-2525	353.229	15.007	1131	0.30	1.67		-1.96			3				
16301-2244	355.343	16.769	1131	0.32	1.66		-1.93			3				
16304-2504	353.553	15.198	1131	0.67	1.54		-1.73			3				
16306-2435	353.975	15.468	1131	0.91	1.01		-1.43			1				
16308-2503	353.629	15.122	1131	0.27	1.63		-2.07			3				
16311-2419	354.255	15.561	1131	0.71	1.26		-1.62			1				
16322-2421	354.392	15.335	1131	0.54	1.29		-1.87			1				
16323-2427	354.328	15.255	1131	0.45	1.47		-1.96			1				
16325-2433	354.276	15.174	1131	0.69	1.52		-1.74			1				
16330-2431	354.383	15.104	2131	0.73	1.26		-1.61			1				
16330-2424	354.472	15.177	1231	0.28	1.44		-1.97			1				
16335-2402	354.844	15.326	1131	0.30	1.47		-1.99			3				
16339-2422	354.646	15.043	1131	0.47	1.21		-1.87			1				
16342-2413	354.801	15.075	1131	0.87	0.98		-1.46			1				
16362-2214	356.693	15.991	1131	0.29	1.24		-2.09			1				
16365-2215	356.728	15.941	1131	-0.02	1.68		-2.32			1				
16367-2356	355.407	14.834	3331	0.43	0.75		-1.31		<1.1	2				
16370-2217	356.769	15.826	1131	0.47	1.20		-1.84			3				
16371-2213	356.840	15.843	1131	0.39	1.25		-2.04			1				
16384-2202	357.184	15.742	1131	-0.14	1.67		-2.35			3				

NOTES:

REFERENCES: (1) IRAS PSC, (2) Weintraub 1990, (3) Gregorio-Hetem et al. 1992, (4) Marquez-Limon, Lopez-Molina, & Chavarria-K 1992, (4A) Wiramihardja et al. 1989, (4B) Wiramihardja et al. 1991, (4C) Wiramihardja et al. 1993, (5) Liseau et al. 1992, (6) Kenyon et al. 1990, (7) Ladd, Lada,& Myers 1993, (8) Myers et al. 1987, (9) Lorenzetti, Spinoglio, & Liseau 1993, (10) Rucinski 1985, (11) Kenyon, Calvet, & Hartmann 1993, (12) Wilking, Lada, & Young 1989, (12A) Lada 1991, (13) Fukui 1989, (14) Wouterloot & Brand 1989, (15) Beichman et al. 1986, (16) Wouterloot & Walmsley 1986, (17) Wouterloot, Brand, & Fiegel 1993, (18) Cesaroni et al. 1988, (19) Palagi et al. 1993, (20) Braz & Scalise 1982, (21) Chini, Krugel, & Kreysa 1986, (22) Bachiller, Martin-Pintado, & Planesas 1991, (23) Morgan, Schloerb, & Snell 1991, (24) Moriarty-Schieven et al. 1992, (25) Wouterloot, Henkel, & Walmsley 1989, (26) Bachiller et al. 1990, (27) Edward & Snell 1984, (28) Roger & Dewdney 1992, (29) McCutcheon et al. 1991, (30) Henning, et al. 1992, (31) Heyer et al. 1990, (32) Leinert & Haas 1989, (33) Zinnecker 1989, (34) Chen et al. 1993, (35) Lada et al. 1991, (36) Tamura et al. 1991, and (37) Strom, Margulis, & Strom 1989.

luminosity at 30–75 μm as $\log (L_{30-75}/L_\odot) = \log L_{60} + 0.15$ (Emerson 1988 b). $\log L_{60}$ is another parameter of the FIR H-R diagram. The lower is logarithm of the FIR luminosity in solar unit obtained by equation (Emerson 1988 b),

$$L_f = 0.31 d^2 (4.578 f_{60} + 1.762 f_{100}) L_\odot. \tag{3}$$

The value is denoted for the first group only.

Column 9: Uncertainty of $\log L_{60}$, obtained from the uncertainty of f_{60}. This column is blank for the second group.

Column 10: The upper is the luminosity ratio of FIR (30 to 135 μm) to mid-infrared (7 to 30 μm) given by Emerson (1988 b), i.e.,

$$L_f/L_m = \frac{(4.578 f_{60} + 1.762 f_{100})}{(20.653 f_{12} + 7.538 f_{25})}. \tag{4}$$

For the first group, the lower limits are shown for the sources with $FQ_{12} = 1$ and/or $FQ_{25} = 1$, while for the second group the upper limits are shown only for the sources with $FQ_{12} \geq 2$ and $FQ_{25} \geq 2$. The L_f/L_m features are indicated in the left panels of Figure 3. The lower is logarithm of mass of the FIR emitting envelope in solar unit. The value is assumed to be 100 times dust mass obtained by equation (5) in §2.3 for $\beta = 1$. The value for $\beta = 2$ is 1.7 times the value for $\beta = 1$. The value is denoted for the first group only.

Column 11: Optical image taken by our inspection and optical counterpart taken from literature; 1 = invisible, 2 = visible star, and 3 = uncertain because there is a very faint star or some field stars or a bright nebula within 1′ of the position of the *IRAS* point source. These features are indicated in Figure 2 and the right panels of Figure 3. The meanings of the additional letters are AE = Herbig Ae/Be star, E = emission line star, N = bright nebula, T = T Tauri star, V = variable star, and wT = weak line T Tauri star. The colon means probable feature.

Column 12: Infrared SED Class taken from literature; 1 = Class I, 2 = Class II, and 2D = Class IID.

Column 13: Active feature taken from literature; H II = H II region, H_2O = H_2O maser, O = CO outflow, and O: = CO wing or broad CO line. The features are indicated in Figure 2 and the right panels of Figure 3.

Column 14: Other name and comment. The comments are IR Neb. = infrared nebulosity, IR Cl. = cluster of infrared stars, Mult. = two or more stars are associated with the *IRAS* point source, and B-ZAMS = B-type zero age main sequence star.

Column 15: Reference for the features cited in Columns 11 to 14 (see footnote of Table 2).

2.2. *FIR H-R Diagrams*

We construct a FIR H-R diagram of YSOs in each star-forming region. The abscissa is the color $\log(f_{100}/f_{60}) \equiv [100\text{–}60]$ and the ordinate is logarithm of the luminosity at 60 μm defined as $\log (d^2 f_{60}) \equiv \log L_{60}$, the values of which are, respectively, listed in Columns 6 and 8 in Table 2.

The FIR H-R diagrams of the six star-forming regions are shown in Figure 3, in which we plotted only the sources belonging to the first group in Table 2 (i.e.,

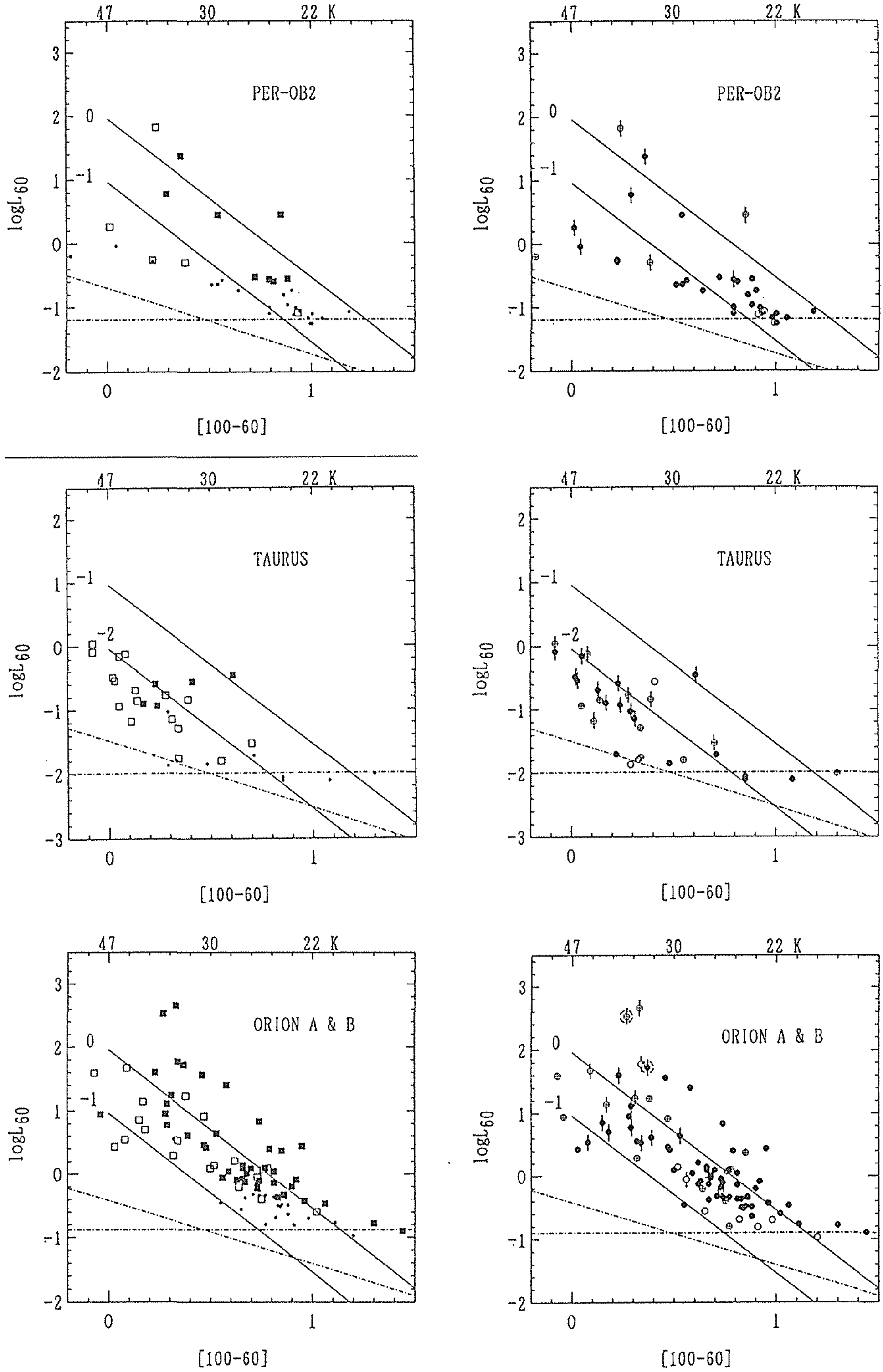

Fig. 3

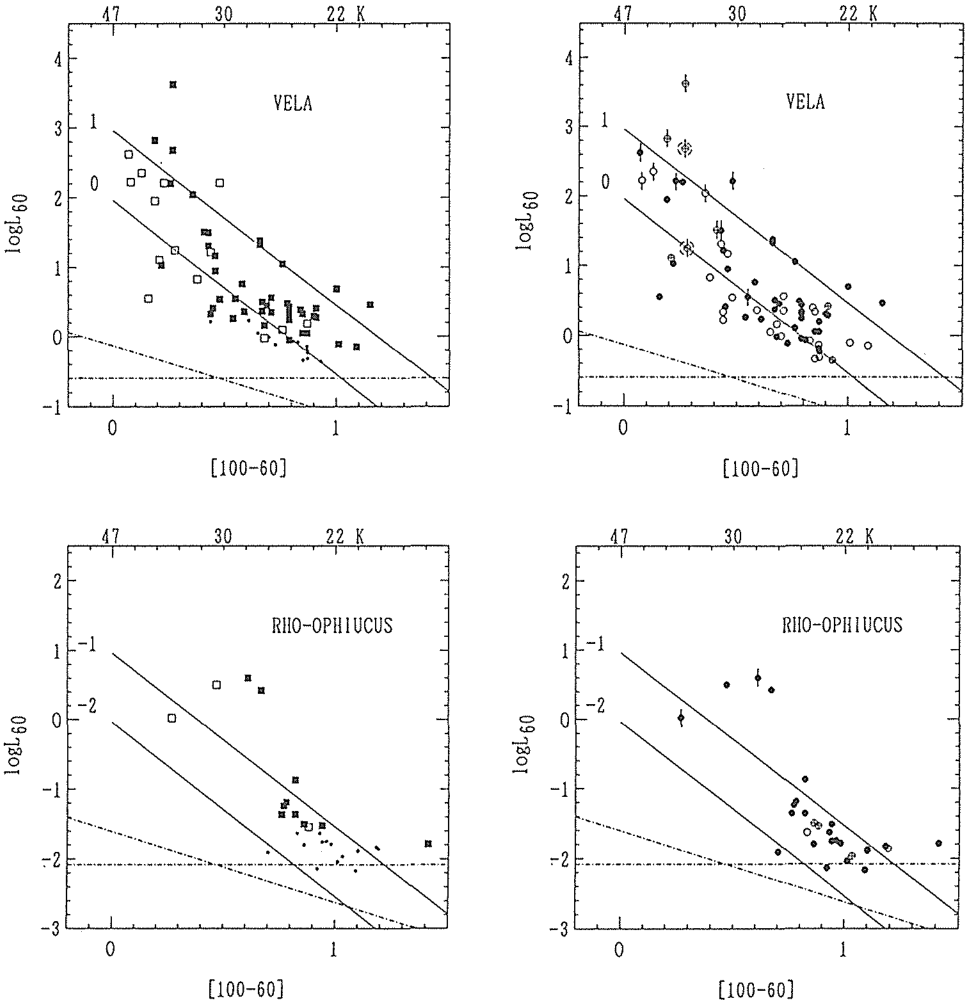

Fig. 3. FIR H-R diagrams of YSOs for the six star-forming regions at distance d kpc; the ordinate is logarithm of the 60 μm luminosity, $\log d^2 f_{60} \equiv \log L_{60}$, and the abscissa is the FIR color, $\log (f_{100}/f_{60}) \equiv [100\text{–}60]$. The L_{60} is related to the luminosity for 30 to 75 μm (Emerson 1988b) as $\log (L_{30\text{–}75}/L_{\odot}) = \log L_{60} + 0.15$. Orion A and B are combined in a diagram. The uncertainties are ≤ 0.20 in [100–60] and ≤ 0.10 in $\log L_{60}$. *The left panels:* The symbols show the luminosity ratio of FIR to mid-infrared, L_f/L_m; the filled squares are the YSOs with $L_f/L_m > 4$ (the extreme Class I YSOs), the open squares are the YSOs with $L_f/L_m < 4$, and the dots are the YSOs whose values of L_f/L_m are uncertain wheter the values are larger than 4. The horizontal dash-dotted line in each diagram represents $f_{60} = 0.5$ Jy, and the inclined line $f_{100} = 1.5$ Jy, which are the *IRAS* sensitivity limits. The solid lines show the constant envelope mass lines and the numbers shown are logarithm of the envelope mass in solar unit (see text). *The right panels:* The same as the left panels, except for the symbols. The filled circles are invisible YSOs, the circles with cross are the YSOs with visible stars, and the open circles indicate the YSOs whose optical counterparts are uncertain. The vertical bars indicate that the objects show the active features such as molecular outflow, H II region, and H_2O maser. The big-dashed circles show the objects associated with infrared cluster.

$FQ_{100} \geq 2$) and having the uncertainties ≤ 0.20 in [100–60] and ≤ 0.10 in $\log L_{60}$ (see Table 2). The YSOs excluded by the uncertainty criteria are 16 in total (6% of the total of the first groups). The error bars in Figure 3 (not indicated) correspond to their mean uncertainties; these are 0.12 in the abscissa and 0.05 in the ordinate. Since the FIR H-R diagrams of Orion A and B are similar to each other, we combine them in a diagram. The color temperatures for $\beta=1$ are indicated on the upper abscissa. The temperature scale for $\beta=2$ shifts by -0.22 in the abscissa. The horizontal dash-dotted lines represent $f_{60}=0.5$ Jy and the inclined ones represent $f_{100}=1.5$ Jy, which are, respectively, the sensitivity limits of the *IRAS* measurements (*IRAS* Explanatory Supplement).

In the left panels of Figure 3, the symbols of plots indicate the luminosity ratio L_f/L_m between the FIR and mid-infrared listed in Columm 10 of Table 2. The filled squares are the YSOs with $L_f/L_m > 4$. In this paper we call those the extreme Class I YSOs, because the YSOs with the spectral index $\alpha=0$ have $L_f/L_m \simeq 1$ and they are still Class I objects. The extreme Class I YSOs are youngest among the selected YSOs. The open squares are the YSOs with $L_f/L_m < 4$ and the dots indicate the YSOs whose values of L_f/L_m are uncertain whether they are larger than 4. In the right panels, the symbols show the optical counterparts and their activities, which are listed in Columns 11 and 13 of Table 2. The filled circles indicate invisible YSOs and the circles with cross are the YSOs associated with visible stars, while open circles indicate the YSOs whose visible features are "uncertain" in our inspection. These features are denoted in Column 11 of Table 2 as 1, 2, and 3, respectively. The associations of visible stars have been also taken from literature (e.g., Weintraub 1990 and others). The circles with vertical bars indicate the objects showing the active features such as molecular outflow (e.g., Fukui 1989), probable embedded outflow (e.g., Wouterloot & Brand 1989), compact H II region, and H_2O maser (e.g., Wouterloot & Walmsley 1986; Palagi et al. 1993). A cross-correlation between the L_f/L_m and optical visibility is shown in Table 3.

About half of the selected YSOs have $FQ_{100}=1$, as shown in Tables 1 and 2. Figure 4 shows the FIR H-R diagram for all of the selected YSOs in Orion A and B, where the circles and crosses indicate the objects with $FQ_{100} \geq 2$ and $=1$, respectively. Most of the objects with $FQ_{100} \geq 2$ have the color [100–60]$=0$ to 1.2, while the objects with $FQ_{100}=1$ tend to have higher color values due to the upper limits of f_{100}. These trends also appear in the FIR H-R diagrams for the other four star-forming regions.

Table 3. Correlation between Optical Visibility and L_f/L_m[1)]

L_f/L_m	>4	<4	Uncertain	<4[2)]
Invisible	86	33	99	25
Visible star	16	25	12	24
Uncertain	21	5	32	5

1) The YSOs, except for those in the last column, are all plotted in the FIR H-R diagrams of Figure 3. 2) The YSOs with $FQ_{100}=1$ in Table 2.

Emerson (1987) deduces that cirrus confusion becomes severe for [100–60]$\gtrsim$0.8. But we found that the mean number of the cirrus flags (CIRR1) for the sources with $FQ_{100}=1$ is not different from that of the sources with $FQ_{100}\gtrsim 2$. We infer that the upper limits of f_{100} are due to the relatively smaller flux densities of the sources. Chen, Tokunaga & Fukui (1993) made *IRAS* co-added images in the Orion A region, the sensitivity of which is 2–3 times higher than that of *IRAS PSC*. They found reliable flux densities at 100 μm for 14 *IRAS* point sources with $FQ_{100}=1$ in Table 2, although their uncertainties are still relatively large. Such YSOs are shown on the FIR H-R diagram in Figure 5, on which the plots for the co-added data are located certainly on the permitted region for the YSOs with $FQ_{100}\gtrsim 2$ in Figure 4. Thus, we consider that the sources with $FQ_{100}\gtrsim 2$ shown in Figure 3 form a sample of cold, bright YSOs in each star-forming region.

Some brightest *IRAS* point sources in each star-forming region are often detected at the central part of infrared clusters, where the projected surface densities of YSOs are up to $\sim 100\ \mathrm{pc}^{-2}$. In Orion A, Strom, Margulis & Strom (1989) showed by a deep 2.2 μm imaging survey that *IRAS* 05338-0624 (L1641-N) contains 20 stellar or semi-stellar objects. *IRAS PSC*'s flag indicates that L1641-N is an extended source both in 12 and 25 μm. In Orion B, Lada et al. (1991 b) found many near-infrared sources in NGC 2023 (*IRAS* 05391-0217) and NGC 2024 (*IRAS* 05393-0156). NGC 2024 is not plotted on the FIR H-R diagram due to its large uncertainty in color [100–60]. Liseau et al. (1992) reported that in Vela, ESO 313-N*10 (*IRAS* 08404-4033) is a cluster of 13 stars and VMR IRS 18 (*IRAS* 08470-4243) a cluster of three stars; the latter is also an

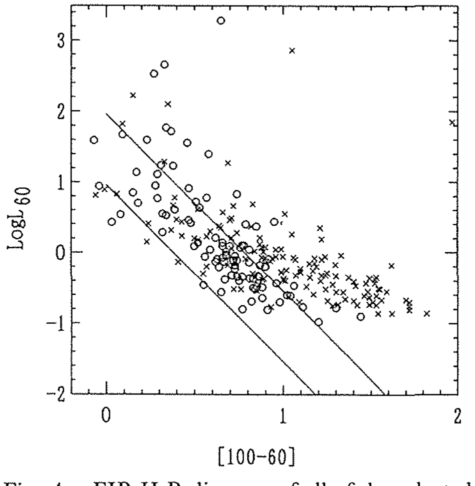

Fig. 4. FIR H-R diagram of all of the selected YSOs in Orion A and B. The circles are the YSOs with reliable flux densities at both 60 and 100 μm, while the crosses are the YSOs with upper limit flux densities at 100 μm.

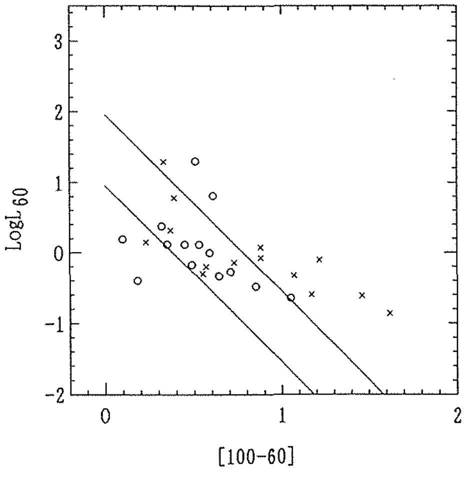

Fig. 5. FIR H-R diagram of 14 YSOs in Orion A. The crosses are plotted by using the data in *IRAS PSC*, the flux densities of which are upper limits at 100 μm. The circles are plotted by using the co-added data of the same objects obtained by Chen et al. (1993) who found the reliable flux densities at 100 μm.

extended source in *IRAS* 12 μm emission. Such *IRAS* point sources thus contain contribution from several or more YSOs. Those sources are indicated by bigger dashed-circles in the right panels of Figure 3 and are excluded from further analysis of the FIR H-R diagram.

2.3. Fundamental Properties of the FIR H-R Diagrams

Dust mass in the FIR emitting envelope is evaluated by assuming that the envelope is optically thin in FIR and the dust is heated by the central source (Hildebrand 1983). Following Hildebrand and WAL, we assume that in envelope the density of dust grains is 3 g cm^{-3}, the grain size 0.1 μm, the dust emissivity $7.5\times10^{-4}\left(\frac{125\,\mu m}{\lambda}\right)^{\beta}$, and the dust grains emit blackbody-like radiation with a temperature T_d at FIR to millimeter wavelengths. Then the dust mass is estimated from the flux density at 60 μm and the dust temperature as

$$M_d = 1.4\times10^{-6}(0.48)^{\beta} d^2 f_{60}(e^{239.8/T_d}-1)M_{\odot}, \qquad (5)$$

where the distance d is in kpc and the flux density f_{60} in Jy. T_d is a function of the color [100–60] and β (see equation (2)). Mass of the FIR emitting envelope, M_{env} is given in Column 10 of Table 2 for each YSO, assuming a gas-to-dust ratio 100 and $\beta=1$. The solid lines in Figure 3 indicate the constant envelope mass. The slope of the line is independent on the values of β and gas-to-dust ratio, and the envelope mass for $\beta=2$ is 1.7 times that for $\beta=1$. Comparing those with WAL's envelope masses, which were derived from the fitting of the spectra from 56 to 3,350 μm of the eleven YSO's, we find a mean mass ratio, $M_{env}/M_{WAL}=\mathrm{dex}\,(-0.06\pm0.23)$.

The spectrum of M_{env} is shown in Figure 6 for each star-forming region, where the fraction of the extreme Class I YSOs (i.e., the YSOs with $L_f/L_m>4$), is illustrated in each bin. The spectrum of L_{FIR} is also shown in Figure 7, where the fraction of the extreme Class I YSOs with active features are indicated in each bin.

The FIR H-R diagrams of Figure 3 are very similar to each other, although the FIR luminosities considerably differ among the star-forming regions, as shown in Figure 7. We recognize the following common properties of the FIR H-R diagrams:

(a) The colors [100–60] of the YSOs range from 0 to 1.2. Especially, the brightest YSOs in each star-forming region are in the range of [100–60]=0 to 0.5.

(b) The active YSOs are most luminous in each star-forming region and its colors [100-60] are less than 0.5, i.e., $45\,\mathrm{K}>T_d>30\,\mathrm{K}$ for $\beta=1$.

(c) In each star forming region, the more luminous YSOs the higher dust temperatures, T_d, as deduced in §1, nearly along the constant "envelope mass" lines. We consider that these lines represent a fundamental sequence on the FIR H-R diagram. We can it *constant envelope mass sequence* (CEMS).

(d) The extreme Class I YSOs (filled squares in the left panels of Figure 3) tend to belong to the higher CEMS. The property is also illustrated in Figure 6, where it is clear that the higher M_{env} has the higher fraction of the extreme Class I YSOs.

(e) The extreme Class I YSOs are mostly invisible. On the other hand, the YSOs with $L_f/L_m<4$ tend to be associated with visible star as compared with the YSOs with $L_f/L_m>4$. The trend is shown in Table 3.

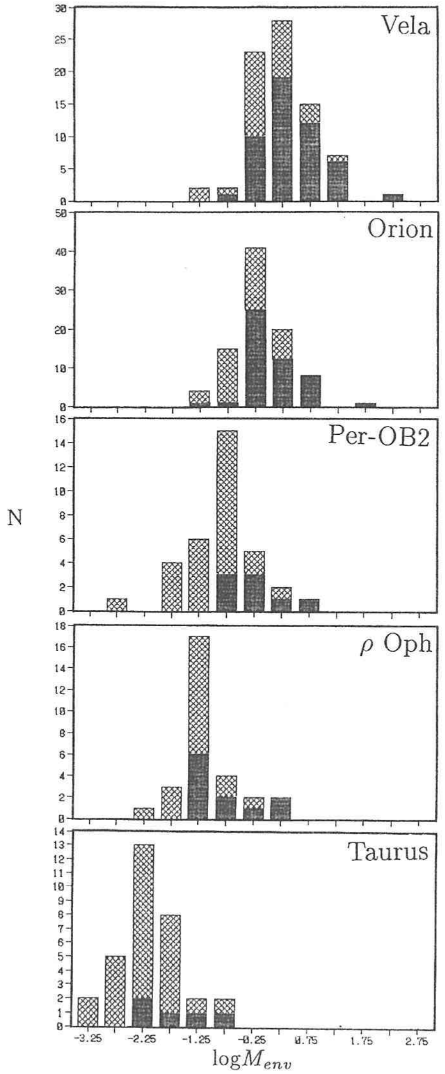

Fig. 6. Distribution of mass of the FIR emitting envelopes for the YSOs plotted in the FIR H-R diagrams (Figure 3). Heavy hatch indicates the YSOs with $L_f/L_m > 4$, i.e., the extreme Class I.

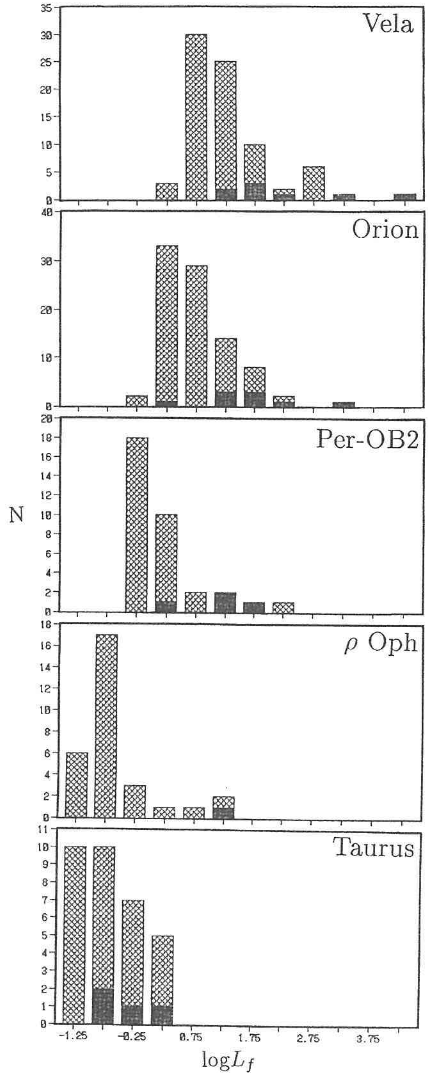

Fig. 7. Distribution of the FIR luminosities for the YSOs plotted in the FIR H-R diagrams (Figure 3). Heavy hatch indicates the extreme Class I YSOs with active features.

The property (a) has been well-known (Beichman et al. 1986; Emerson 1987; Wouterloot, Walmsley & Henkel 1988). The property (b) has been also recognized. The active YSOs are most luminous in the individual star-forming regions (e.g., Fukui 1988; Myers et al. 1988; Snell at al. 1988; Cabrit & André 1991; Chen et al. 1993). The *IRAS* point sources with CO outflows are listed in Berrili et al. (1989) and Fukui (1989); the luminosities mostly range in $1-10^5 L_\odot$ and the average value and standard deviation of the colors [100–60] are 0.18 ± 0.22 for 31 sources with reliable *IRAS* flux densities in the former sample and 0.27 ± 0.19 for 102 sources in the latter sample.

Wood & Churchwell (1989) find the *IRAS* color [100–60] of 30 ultracompact H II regions to be 0.26 ± 0.14. Wouterloot & Walmsley (1986) show that *IRAS* sources with H_2O masers mostly have [100–60]=0 to 0.6. The properties (c)–(e) have been partly recognized in relation with YSOs evolution, as shall be shown in §3.2.

Besides the similarities mentioned above, we also notice the following differences among the FIR H-R diagrams of the individual clouds, which are mainly related to the YSOs masses and their evolutionary stages:

(i) The FIR luminosities L_f and the masses M_{env} of the FIR emitting envelopes: The difference of these values among the star-forming regions are clearly seen in Figures 6 and 7; the peaks of both the $\log M_{env}$ and $\log L_f$ spectra become less in order of the Vela, Orion, Per-OB2, ρ-Ophiucus, and Taurus. The peak values are listed in Table 4 and plotted by open squares in Figure 8; both the values, except for Taurus, are proportional to each other in an order of 1.5, i.e., $(M_{env}, L_f) = (1.8M_\odot, 5.6L_\odot)$ in Vela to $(0.056M_\odot, 0.18L_\odot)$ in ρ-Ophiucus. For Taurus, the deviation from the correlation may be due to the higher fraction of evolved YSOs, i.e., the lower fraction of the extreme Class I YSOs (see Figure 6). We consider that the median of M_{env} for the extreme Class I YSOs in each star-forming region represents a typical M_{env} of the highest-mass YSOs in that region, and the median of L_f for the active extreme Class I YSOs corresponds to a typical luminosity in the most luminous phase of such YSOs. These values are also listed in Table 4 and plotted in Figure 8 (filled squares), except for ρ-Ophiucus. These $\log M_{env}$ and $\log L_f$ decrease nearly linearly from Vela to Taurus, i.e., $(M_{env}, L_f) = (2.5M_\odot, 158L_\odot)$ in Vela to $(0.01M_\odot, 0.3L_\odot)$ in Taurus.

(ii) The fraction of extreme Class I YSOs: In Taurus the fraction is clearly less

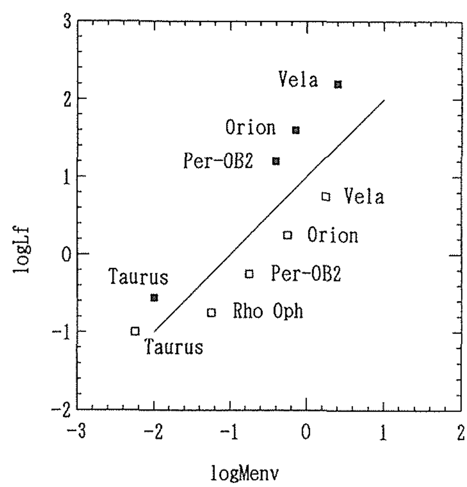

Fig. 8. Open squares: a correlation between the peaks of distributions of the envelope mass and FIR luminosity of YSOs. The mass and luminosity are in solar units. Filled squares: a correlation between the median of envelope masses of the extreme Class I YSOs and the median of the FIR luminosities of the active extreme Class I YSOs. The line indicates $L_f = 10M_{env}$ in solar units.

Table 4. Characteristic FIR Luminosity and Envelope Mass of YSOs in the Five Star-Forming Regions[1)]

	Per-OB2	Taurus	Orion	Vela	ρ-Oph
$\log L_f$ at peak	−0.25	−1.0	0.25	0.75	−0.75
$\log M_{env}$ at peak	−0.75	−2.25	−0.25	0.25	−1.25
γ index of mass spectrum	−1.8	−1.6	−1.7	−1.6	−1.6
Fraction of extreme Class I	0.24	0.16	0.54	0.63	0.38
Median of $\log L_f$[2)]	1.2 (4)	−0.56 (4)	1.6 (9)	2.2 (8)	1.2 (1)
Median of $\log M_{env}$[3)]	−0.4 (8)	−2.0 (5)	−0.15 (48)	0.4 (49)	−1.1 (11)
γ index of mass spectrum[3)]	—	—	−1.5	−1.5	—

1) See Figures 6 and 7. The luminosity and mass are in solar units. 2) For the extreme Class I YSOs with active features. The numbers in paranthesis are the YSOs' number. 3) For the extreme Class I YSOs. The numbers in parathesis are the YSOs' number.

than in the other star forming regions (see Figure 6 and Table 4). This difference must be related to the evolutionary stage of star formation in the individual clouds. But the statistics in each star-forming region are imcomplete due to existence of many YSOs with $FQ_{100}=1$ (the second group of Table 2) and probably many colder YSOs with $FQ_{60}=1$ and $FQ_{100}\geq 2$ which are not taken into account in this study.

3. Discussion

3.1. Mass of the FIR Emitting Envelope

The mass spectrum of molecular cores in a star-forming region has an index between −1.7 and −1.4, which are different from the index of stellar mass of −2.35 (Blitz 1991 ; Tatematsu et al. 1993). The mass spectra of the FIR emitting envelope shown in Figure 6 have indexes of $\gamma=-1.8$ to -1.6 (see Table 4). The indexes are also evaluated for the mass spectra of the extreme Class I YSOs in Orion and Vela and their values are both $\gamma=-1.5$. Those are similar to the indexes of molecular cores.

Chen et al. (1993) measured column densities of $^{13}CO(J=1-0)$ with a beam size of 2.7′ on *IRAS* point sources in Orion A. They also obtained the *IRAS* flux densities by making co-added images. By using their flux densities at 60 μm and 100 μm with the uncertainties less than 50%, we found values of [100−60], L_{60}, L_f/L_m, and M_{env} of the point sources. We illustrate in Figure 9 the correlation between the M_{env} and $N(^{13}CO)$ for the sources with $N(^{13}CO)>0.4\times10^{16}$ cm^{-2}. Figure 9 shows that M_{env} of the YSOs with $L_f/L_m>4$ increase with $N(^{13}CO)$, while the YSOs with $L_f/L_m<3$ deviate from this correlation which must be due to decreasing of dust mass and molecular mass with evolution. The correlation seems to be $N(^{13}CO)\propto M_{env}^{0.6}$. The molecualr core masses of three objects in Figure 9 were derived by Chen, Fukui & Yang (1992) and the masses are several times larger than M_{env}.

We show in Figure 10 a correlation between M_{env} and L_f for the YSOs plotted in all of the FIR H-R diagrams of Figure 3. We find in this diagram that the more luminous YSOs which are making higher mass stars tend to have the higher envelope mass, but the sequence of the YSOs with $L_f/L_m>4$ (filled squares) separates from that of the

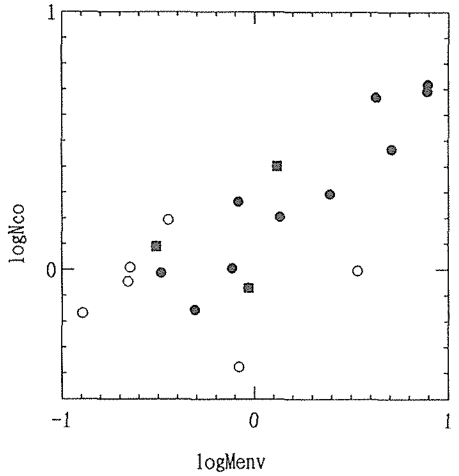

Fig. 9. A correlation between mass, $M_{env}(M_\odot)$, of the FIR emitting envelope and ^{13}CO (J=1–0) column density in unit of 10^{16} cm^{-2}, $N(^{13}CO)$, of YSOs in Orion A. The $N(^{13}CO)$ were obtained by Chen et al. (1993) in a 2.7′ beam size. The filled circles indicate YSOs with $L_f/L_m>4$, filled squares YSOs with $L_f/L_m>3$, and the open circles YSOs with $L_f/L_m<3$.

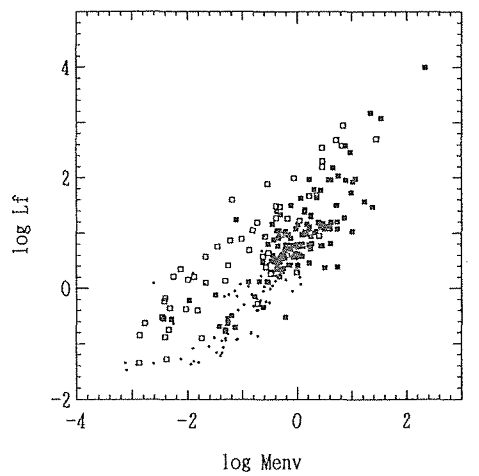

Fig. 10. A correlation between the envelope mass and the FIR luminosity for the individual YSOs plotted in the FIR H-R diagrams (Figure 3). The filled squares are YSOs with $L_f/L_m>4$, the open squares YSOs with $L_f/L_m<4$, and the dots YSOs with unknown L_f/L_m value.

YSOs with $L_f/L_m<4$ (open squares). The YSOs move from the lower sequence to the upper one as they are evolving. As shown in the mass spectrum of each star forming region in Figure 6, the YSOs decrease the envelope mass by a half to one order of magnitude with evolution from the phase of $L_f/L_m>4$ to <4. If the decreasing of L_f also occurs with a rate similar to that of M_{env}, the separation of sequences in Figure 10 is not realized. If M_{env} decreases without decreasing of L_f, the separation between the two sequences in Figure 10 means that the M_{env} decrement is about one order of magnitude for YSOs with $L_f\sim 1L_\odot$ to $10L_\odot$, and the rate seems to be less for the YSOs with higher L_f. This is consistent with the results deduced from the mass spectrum of each star-forming region. André & Montmerle (1994) found a similar trend from their 1.3 mm observations of YSOs in ρ-Ophiucus.

Assuming that the resulting stellar mass is $\sim 0.5M_\odot$ in Taurus and $\sim 4M_\odot$ in Orion and the typical envelope masses are the medians of the extreme YSOs shown in Table 4, we obtain $M_{env}/M_{star}\sim 0.02$ and ~ 0.2 for YSOs in Taurus and Orion, respectively. Since $M_{env}/M_{star}<1$ even at the extreme Class I stage, these YSOs seem to have already stored materials of stellar mass at the central parts in this evolutionary stage (André & Montmerle 1994).

3.2. Evolutionary Sequence

The FIR H-R diagram describes the evolutionary sequence of YSOs which are usually accepted based on many observational and theoretical works. The birth of protostars begins by infalling of inner part of molecular cloud cores. The main feature at this first stage is the increasing of luminosity and the growing of central objects (star+disk). The radiation is emitted mainly at FIR wavelength. This evolutionary sequence of YSOs is represented by the CEMS on the FIR H-R diagram, i.e., the common property (c) ; the YSOs move upward along the CEMS with increasing the 60 μm luminosity, raising the temperature of the envelope, and keeping the mass of the FIR emitting envelope nearly constant. The increase of mass and luminosity of the central objects induce at last the activities such as molecular outflow, H_2O maser, and compact H II region (the common property (b) of the FIR H-R diagrams). During and after the active phase, the (dust) mass of the FIR emitting envelope reduces and the SEDs of YSOs extend toward mid- and near-infrared wavelengths as well as decreasing the FIR luminosities, and the central stars become visible. The trends appear in the FIR H-R diagrams as the common properties (d) and (e).

To delineate specifically the evolutionary sequence in the early, pre-active stage and also post-active stage, we examine the FIR H-R diagram of each star-forming region (Figure 3) using other observational data of YSOs.

Per-OB2

In the Per-OB2 both low- and high-mass stars have formed (Bachiller, Martin-Pintado & Planesas 1991 ; Ladd et al. 1993). This appears also in the FIR H-R diagram in Figure 3. The five luminous sources with $\log L_{60}>0.4$ are the high-mass YSOs with $M_{env}\sim 1M_\odot$, while the others are low-mass YSOs. The three luminous YSOs, SVS 3 at ([100−60], $\log L_{60}$)=(0.24, 1.82), RNO 15 FIR at (0.29, 0.77) and L1448 IRS3 at (0.85, 0.45), are associated with H II regions (references are shown in Table 2). RNO 15 FIR shows a CO outflow with "age" 2.2×10^4 yr (Fukui 1989 and references therein). Roger & Dewdney (1992) suggest that SVS3 is B3.5 ZAMS. L1448 IRS3 is B3 ZAMS with outflow of "age" $\sim3.5\times10^3$ yr (Anglada et al. 1989 ; Bachiller et al. 1990). Their M_{env}/M_{star} are thus ~0.2–0.3.

Bachiller et al. (1991) found outflows in IRAS 03271+3013 and 03282+3035 associated with T Tauri stars (TTSs) (~2–3$M_\odot$) ; the latter is located at (0.79, −0.57), and the outflow is young ($\sim1.6\times10^4$ yr) and unusual jet-like ($v\sim70$ km/s). About ten YSOs with $M_{env}\sim0.1M_\odot$ and $\log L_{60}<-0.5$ are mostly invisible and probably the extreme Class I YSOs ; they may be young, except for a TTS LkH-α 325 at (0.93, −1.09). The YSOs with $M_{env}<0.1M_\odot$ and $T_d>30$ K for $\beta=1$, on the other hand, tend to have $L_f/L_m<4$, and they are older. One of these is a TTS RNO 13 at (0.38, −0.30) showing an outflow with "age" 2.3×10^4 yr (Fukui 1989 and references therein).

Tauras

In the Taurus star-forming region, the YSOs luminosities at FIR are mostly lower than those in Per-OB2 (see Figure 7). T Tauri stars have masses less than $1M_\odot$ in Taurus (Beckwith et al. 1990) and ~2–3$M_\odot$ in Per-OB2 (Bachiller et al. 1991). The FIR H-R diagram indicates that most of the YSOs in Taurus have $L_f/L_m<4$ and the fraction of visible stars is higher than in Per-OB2. Furthermore, the selected YSOs with $FQ_{100}=1$ in Taurus (the second group in Table 2) are mostly the TTSs with the Class II SEDs. Thus, the YSOs in Taurus are in the later evolutionary stages than those in Per-OB2.

The embedded YSO (IRAS 04368+2557) assciated with L1527 is at (0.61, −0.46) on the FIR H-R diagram and presumably the youngest active YSO in our sample of the Taurus. The value of $L_f/L_m > 19.5$ is very large and its SED shows a single peak modified blackbody for $T = 30$ K with $L_{FIR} = 1.8 L_\odot$ (Ladd et al. 1991). L1527 is a dense NH_3 core with a radius of 0.08 pc and a core mass of 2.4 $M_\odot$ (Benson & Myers 1989). The core mass is ~20 times larger than the M_{env}, implyng that the molecular core radius is one order of magnitude larger than that of the FIR emitting region.

Ohashi et al. (1991) detected CS ($J = 2-1$) emission associated with L1527 and also the bright YSOs with the higher dust temperatures, IRAS 04169+2702 at (0.02, −0.49), IRAS 04240+2559 (DG Tau) at (0.08, −0.12), and IRAS 04361+2547 (TMR-1) at (−0.08, −0.09), but not detected for the less bright TTSs, IRAS 04189+2650 (FS Tau) and 04306+2514 (DL Tau) with $\log L_{60} = -0.86$ and −1.55, respectively.

Table 5. T Tauri Stars with Similar Mass in Taurus

TTs	IRAS Name	[100–60]	$\log L_{60}$	$\log L_f$	$\log M_{env}$	$M_*(M_\odot)$ [1]	log (age) [1]
DG Tau	04240+2559	0.08	−0.12	0.20	−1.88	0.56	5.47
Haro 6–13	04292+2422	0.14	−0.85	−0.52	−2.46	0.55	5.10
HK Tau	04288+2417	0.34	−1.29	−0.88	−2.40	0.55	5.94
DP Tau	04395+2509	0.55	−1.80	−1.28	−2.38	0.60	6.20

1) Star's mass in solar unit and age in year of Beckwith et al. (1990).

The mean ages of TTSs of Beckwith et al. (1990) are 9.2×10^5 yr for three TTSs with color [100−60]>0.3 and 7.9×10^5 yr for five TTSs with color [100−60]<0.3. Especially, when we compare four TTSs with similar stellar mass in Table 5, the positions of three TTSs on the FIR H-R diagram move with age toward larger [100−60] and lower log L_{60}. These facts suggest an evolutionary path of the TTSs stage on the FIR H-R diagram that both the 60 μm luminosity and the dust temperature of the envelope decrease along the lower CEMS.

There is other observational evidence supporting this trend on the evolutionary path of pre-main sequence stars. Clark (1991) examined 205 nearby *IRAS* point sources, which are thought to be pre-main sequence stars, and found that in accordance with increasing of the separation from the molecular core, presumably with age (Myers et al. 1987), the colors [100–60] increase from 0.2 to 0.85 and the infrared luminosities decrease about one order of magnitude. Beckwith et al. (1990) find from the 1.3 mm continuum emission of TTSs that the circumstellar dust masses do not decrease with age up to 10^7 yr. They also show that the 60 μm flux densities decrease with decreasing dust temperature and the older TTSs tend to have lower dust temperatures. Beckwith et al. (1990) and Clark (1991) suggest the reasons of these trends as due to decreasing of their luminosity and their energetic activity, such as accretion, with time.

Orion

There are two brightest YSOs with $\log L_{60}>2$; one is IRAS 05391-0217 (NGC 2023) which is an infrared cluster and an extended source in $100\,\mu$m emission, and another is IRAS 05327-0457 which is probably the most massive YSO in our sample. Excluding the two objects, the YSOs in the FIR H-R diagram seem to be divided into two groups by M_{env}. Wiramihardja et al. (1991) show that both high- and low-mass YSOs co-exist in the Orion cloud.

The YSOs along the CEMS of $M_{env}\sim 5M_{\odot}$ are the extreme Class I and thus are in early evolutionary stage. The brightest of these is NGC 2068 H_2O at (0.34, 1.77) which has an outflow with the "age" of 2×10^5 yr (Edwards & Snell 1984). IRAS 05335-0645 at (0.85, 0.37) is associated with three TTSs (Weintraub 1990), but it has a high L_f/L_m (>8.1). Around the CEMS of $M_{env}\sim 1M_{\odot}$, there are five visible YSOs with $L_f/L_m\lesssim 4$ (open squares on the left panel). One of these YSOs is a Herbig Ae/Be star N'SK 81 at (0.78, 0.10). Those YSOs are probably high-mass YSOs evolved from the extreme Class I YSOs with $M_{env}\sim 5M_{\odot}$.

There are many invisible extreme Class I YSOs around the CEMS of $M_{env}\sim 1M_{\odot}$, while the YSOs with $L_f/L_m<4$ are distributed nearly along the CEMS of $M_{env}\sim 0.2M_{\odot}$. One of the visible YSOs, IRAS 05464+0106 at (0.64, −0.21), is a TTS (Gregorio-Hetem et al. 1992), and three other visible YSOs around the CEMS of $M_{env}\sim 0.2M_{\odot}$ are likely to be TTSs (Wiramihardja et al. 1991, 1993). These TTSs are probably YSOs evolved from the extreme Class I YSOs with $M_{env}\sim 1M_{\odot}$.

Vela

On the left panel in Figure 3, the extreme Class I YSOs (filled squares) are distributed along the CEMS of $\sim 10M_{\odot}$ and $\sim 1M_{\odot}$. These are high-mass YSOs in the early evolutionary stage. The most massive group contains a Herbig Ae/Be star RCW 34 at (0.19, 2.82) which is associated with H II region, bright nebula and H_2O maser. The brightest YSOs inVela, IRAS 08576-4334 at (0.27, 3.62) is associated with a Herbig Ae/Be star, H II region, bright nebula, H_2O maser and probable outflow RCW 36; this is an extended source at the *IRAS* four bands and probably a complex of massive YSOs. Liseau et al. (1992) claim that the most massive stars in the Vela star-forming region are the early B-type. Thus the M_{env}/M_{star} is close to unity for such massive stars.

ρ-Oph

The YSOs in this star-forming region are mostly less luminous and have cold envelopes. The envelope masses are larger than YSOs in Taurus (see also Figure 6) but the FIR luminosites are similar to YSOs in Taurus (see Figure 7). Kenyon et al. (1990) show that the luminosity function for Class I and Class II sources in ρ-Oph is similar to that in Taurus-Aurigae, but the fraction of Class I sources is larger in ρ-Oph than in Tau-Aur. These also suggest that M_{env} of low-mass YSOs reduces by one order of magnitude during the evolution from the extreme Class I stage to TTS stage.

The two brightest YSOs with $\log L_{60}>0.4$ seem to be more massive than others. One of these IRAS 16293-2422 (ρ-Oph-S) at (0.61, 0.60) has $L_f/L_m>158$ which is the largest value in our sample of YSOs listed in Table 2. For this YSO, André et al. (1990) obtained $M_{env} \sim 0.41 M_{\odot}$ from the observation at 1.3 mm, and Wilking et al. (1989) give the infrared emitting mass to be 2 $M_{\odot}$. Lada (1991, and reference therein) showed that its SED fits a single temperature modified blackbody ($T=35$ K for $\beta=1.5$), and suggested that the YSO is associated with edge-on bipolar outflows.

In the four FIR H-R diagrams, except for that of Taurus, the extreme Class I YSOs are more at [100–60] > 0.5 than at [100–60] < 0.5. The trend implies that the life time in the cold, less luminous extreme Class I YSOs stage is comparable to or rather longer than that in the luminous active phase. This result differs from that of the spherical symmetric infalling model (e.g., Yorke 1979; Stahler et al. 1980), and supports the model that the gas accretion onto the central star slowly occurs through the circumstellar disk (Terebey at al. 1984; Shu et al. 1987).

4. Summary

The FIR H-R diagrams of YSOs are constructed for each of six nearby star-forming regions by using the *IRAS* flux densities at 60 and 100 μm. The FIR H-R diagrams are characterized by a constant envelope mass sequence (CEMS) along which YSOs change the dust temperatures in the envelope in accordance with the luminosities of the central objects keeping the envelope mass and radius nearly constant.

The evolution of the YSOs is traced along the CEMS; (1) in the early phase YSOs, i.e., the extreme Class I YSOs, move upward along the CEMS with increasing the luminosity of the central object and the dust temperature of the envelope, (2) the YSOs become active at the brightest phase and reduce the mass of envelope, and (3) after the active phase the FIR luminosity decreases with time and the dust temperature of the envelope becomes lower, i.e., the YSOs move downward along the lower CEMS.

Analyzing the FIR H-R diagrams of the nearby star-forming regions, we suggest the extreme Class I YSOs have already stored most of the material of stellar mass at the central part and are forming stars by a slow accretion of the material.

We may use the FIR H-R diagrams to specify the evolutionary state of a YSO and the resulting stellar mass. The FIR H-R diagrams must be made in future by FIR observations with higher sensitivity and spatial resolution for many other star-forming regions.

One of us (TD) thanks the Japanese Ministry of Education, Science, and Culture for the scholarship.

References

Adams, F.C., *ApJ*, **363**, 578, 1990.
Adams, F.C. and Shu, F.H., *ApJ*, **296**, 655, 1985.
Adams, F.C., Lada, C.J. and Shu, F.H., *ApJ*, **312**, 788, 1987.
André, P. and Montmerle, T., *ApJ*, **420**, 837, 1994.
André, P., Montmerle, T., Feigelson, E.D. and Steppe, H., *A&A*, **240**, 321, 1990.
Anglada, G., Rodriguez, L.F., Torrelles, J.M., Estalella, R., Mo, P.T.P., Canto, J., Lopez, R. and

Verdes-Montenegro, H., *ApJ*, **341**, 208, 1989.
Bachiller, R., Cernicharo, J., Martin-Pintado, J., Tafalla, M. and Lazareff, B., *A & A*, **231**, 174, 1990.
Bachiller, R., Martin-Pintado, J. and Planesas, P., *A & A*, **251**, 639, 1991.
Beckwith, S., Sargent, A.I., Scoville, N.Z., Masson, C.R., Zuckerman, B. and Phillips, T.G., *ApJ*, **309**, 755, 1986.
Beckwith, S.V.W., Sargent, A.I., Chini, R.S. and Guesten, R., *AJ*, **99**, 924, 1990.
Beichman, C.A., Myers, P.C., Emerson, J.P., Harris, S. Mathieu, R., Benson, P.J. and Jenning, R.E., *ApJ*, **307**, 337, 1986.
Benson, P.J. and Myers, P.C., *ApJS*, **71**, 89, 1989.
Berrili, F., Ceccarelli, C., Liseau, R., Lorenzetti, D., Saraceno, P. and Spinoglio, L., *MNRAS*, **237**, 1, 1989.
Blitz, L. in The Physits of Star Formation and Early Stellar Evolutirn, eds. C.J. Lada & N.D. Kylafis (Dorbrecht: Kluwwer), p. 3, 1991.
Braz, M.A. and Scalise, Jr., E., *A & A*, **107**, 272, 1982.
Butner, H.M., Evans II, N.J., Harvey, P.M., Mundy, L.G., Natta, A. and Randich, M.S., *ApJ*, **364**, 164, 1990.
Carbrit, S. and André, P., *ApJ*, **379**, 125, 1991.
Carpenter, J.M., Snell, R.L., Schloerb, F.P. and Skrutskie, M.F., *ApJ*, **407**, 657, 1993.
Cesaroi, R., Palagi, F., Feli, M., Catarzi, M., Comoretto, G., Di Franco, S., Giovanadri, C. and Palla, F., *A & AS*, **76**, 445, 1988.
Chen, H., Fukui, Y. and Yang, J., *ApJ*, **398**, 544, 1992.
Chen, H., Tokunaga, A.T. and Fukui, Y., *ApJ*, **416**, 235, 1993.
Chen, H., Tokunaga, A.T., Strom, K.M. and Hodapp, K.W., *ApJ*, **407**, 639, 1993.
Chini, R., Kresa, E., Mezger, P.G. and Gemund, H.P., *A & A*, **154**, L8, 1986.
Chini, R., Krügel, E. and Kreysa, E., *A & A*, **167**, 315, 1986.
Churchwell, E., Wolfire, M. G. and Wood, D.O.S., *ApJ*, **354**, 247, 1990.
Clark, F.O., *ApJS*, **75**, 611, 1991
Dame, T.M., Ungerechts, H., Cohen, R.S., de Geus, E.J., Grenier, I.A., Ma, J., Murphy, D.C., Nyman, L.-A. and Thaddeus, P., *ApJ*, **322**, 706, 1987.
Davidson, J.A., *ApJ*, **315**, 602, 1987.
de Geus, E.J., Bronfman, L. and Thaddeus, P., *A & A*, **231**, 137, 1990.
Edwards, S. and Snell, R.L., *ApJ*, **281**, 237, 1984.
Ellis, Jr., H.B., Lester, D.F., Harvey, P.M., Joy, M., Telesco, C.M, Decher, R. and Werner, M.W., *ApJ*, **365**, 287, 1990.
Emerson, J.P., in Star Forming Regins, eds, M. Peimbert and J. Jugaku (Drdrecht: D. Reidel), p.19, 1987.
Emerson, J.P., in Formation and Evolution of Low Mass Starss, eds. A.K. Dupree and M.T.V.T. Lago (Dordrecht: Kluwer), p. 21, 1988a.
Emerson, J.P., in Formation and Evolution of Low Mass Starss, eds. A.K. Dupree and M.T.V.T. Lago (Dordrecht: Kluwer), p. 193, 1988b.
Fukui, Y., *Vistas Astron.*, **31**, 217, 1988.
Fukui, Y., in Low Mass Star Formation and Pre-Mains Sequence Objects, ed. Bo Reipurth, (ESO, Garching), p. 95, 1989.
Gregorio-Hetem, J., Lepine, J.R.D., Quast, G.R., Torres, C.A.O. and de la Rea, R., *AJ*, **103**, 549, 1992.
Gürtler, J. Henning, Th., Krügel, E and Chini, R., *A & A*, **252**, 801, 1991.
Harris, S., Clegg, P. and Hughes, J., *MNRAS*, **235**, 441, 1988.
Harvey, P.M., Thronson, Jr., H.A. and Gatley, I., *ApJ*, **231**, 115, 1979.
Henning, T., Cesaroni, R., Walmsley, M. and Pfau, W., *A & AS*, **93**, 525, 1992.
Heyers, M.H., Ladd, E.F., Myers, P.C. and Campbell, B., *AJ*, **99**, 1585, 1990.
Hildebrand, R.H. *QJRAS*, **24**, 267, 1983.
IRAS Explanatory Supplement, eds. C.A. Beichman, G. Neugebauer, H.A.J. Habing, P.E. Clegg and T.J. Chester (Washington, DC: NASA), 1988.
IRAS Point Sources Catalog, Version 2.0, in Selected Astronomical Catalogs Vol. 1 (CD-ROM),

Astronomical Data Center, NASA, 1986.
Kenyon, S.J., Calvet, N. and Hartmann, L., *ApJ*, **414**, 676, 1993.
Kenyon, S.J., Hartmann, L.W., Strom, K.M. and Strom, S.E., *AJ*, **99**, 869, 1990.
Lada, C.J., in Star Forming Regions, eds. M. Peimbert and J. Jugaku (Dordrecht: D. Reidel), p. 1, 1987.
Lada, C.J., in The Physics of Star Formation and Early Stellar Evolution, eds. C.J. Lada and N.D. Kylafis (Dordrecht: Kluwer), p. 329, 1991.
Lada, E.A., Bally, J. and Stark, A.A., *ApJ*, **368**, 432, 1991 a.
Lada, E.A., DePoy, D.L., Evans II, N.J. and Gatley, I., *ApJ*, **371**, 171, 1991 b.
Ladd, E.F., Adams, G.C., Casey, S., Davidson, J.A., Fuller, G.A., Harper, D.A., Myers, P.C. and Padman, R., *ApJ*, **366**, 203, 1991.
Ladd, E.F., Lada, E.A. and Myers, P.C., *ApJ*, **410**, 168, 1993.
Larson, R.B., in Star Formation, ed. T. De Jong and Maeder, p. 249, 1977.
Leinert, C. and Haas, M., *ApJ*, **342**, L39, 1989.
Liseau, R., Lorenetti, D., Nisini, B., Spinoglio, L. and L. Monetti, A., *A&A*, **265**, 577, 1992.
Lorenzetti, D., Spinoglio, L. and Liseau, R., *A&A*, **275**, 489, 1993.
Maddalena, R.J., Morris, M., Moscowitz, J., and Thaddeus, P., *ApJ*, **303**, 375, 1986.
Márque-Limon, A., Lopéz-Molina, M.G. and Chavarria-K, C., *A&AS*, **95**, 391, 1992.
McCutcheon, W.H., Dewdney, P.E., Purton, C.R. and Sato, T., *AJ*, **101**, 1435, 1991.
Mezger, P.G., Wink, S.E., Zylka, R., *A&A*, **228**, 95, 1990.
Morgan, J.A., Schloerb, F.P. and Snell, R.L., *ApJ*, **376**, 618, 1991.
Moriarty-Schieven, G.H., Wannier, P.G., Tamura, M. and Keene, J., *ApJ*, **400**, 260, 1992.
Myers, P.C., Fuller, G.A., Mathieu, R.D., Beichman, C.A., Benson, P.J., Schild, R.E. and Emerson, J.P., *ApJ*, **319**, 340, 1987.
Myers, P.C., Heyer, M., Snell, R.L. and Goldsmith, P.F., *ApJ*, **324**, 907, 1988.
Myers, P.C. and Ladd, E.F., *ApJ*, **413**, L47, 1993.
Natta, A., Palla, R., Butner, H.M., Evans II, N.J. and Harvey, P.M., *ApJ*, **406**, 674, 1993.
Ohashi, N., Kawabe, R., Hayashi, M. and Ishiguro, M., *AJ*, **102**, 2054, 1991.
Palagi, F., Cesaroni, R., Comoretto, G., Felli, M. and Natale, V, *A&AS*, **101**, 153, 1993.
Roger, R.S. and Dewdney, P.E., *ApJ*, **385**, 536, 1992.
Rowan-Robinson, M., *ApJS*, **44**, 403, 1980.
Rucinski, S.M., *AJ*, **90**, 2321, 1985.
Sargent, A.I., *ApJ*, **233**, 164, 1979.
Scoville, N.Z. and Kwan, J., *ApJ*, **206**, 718, 1976.
Shu, F.H., *ApJ*, **214**, 488, 1977.
Shu, F.H., Adams, F.C. and Lizano, S., *ARA&A*, **25**, 23, 1987.
Snell, R.L., Huang, Y.L., Robert, L., Dickman, L. and Claussen, M.J., *ApJ*, **325**, 853, 1988.
Stahler, S.W., Shu, F.H. and Taam, R.E., *ApJ*, **241**, 637, 1980.
Strom, K.M., Margulis, M. and Strom, S.E., *ApJ*, **346**, L33, 1989.
Strom, K.M., Strom, S.E. and Merrill, K.M., *ApJ*, **412**, 233, 1993.
Tamura, M., Gatley, I., Waller, W. and Wernen, M.W., *ApJ*, **374**, L25, 1991.
Tatematsu, K., Umemoto, T., Kaneya, O., Hirano, N., Hasegawa, T., Hayashi, M., Iwata, T., Kaifu, N., Mikami, H., Murata, Y., Nakano, M., Nakano, T., Ohashi, N., Sunada, K., Takaba, H. and Yamamoto, S., *ApJ*, **404**, 643, 1993.
Terebey, S., Shu, F.H. and Cassen, P., *ApJ*, **286**, 529, 1984.
Ungerechts, H. and Thaddeus, P., *ApJS*, **63**, 645, 1987.
Walker, C.K., Adams, F.C. and Lada, C.J., *ApJ*, **349**, 515(WAL), 1990.
Weintraub, D.A., *ApJS*, **74**, 575, 1990.
Wilking, B.A., Lada, C.J. and Young, E.T., *ApJ*, **340**, 823, 1989.
Wilking, B.A., Mundy, L.G., Blackwell, J.H. and Howe, J.E., *ApJ*, **345**, 257, 1989.
Wiramihardja, S.D., Kogure, T., Yoshida, S., Ogura, K. and Nakno, M., *PASJ*, **41**, 155, 1989.
Wiramihardja, S.D., Kogure, T., Yoshida, S., Nakano, M., Ogura, K. and Iwata, T., *PASJ*, **43**, 27, 1991.
Wiramihardja, S.D., Kogure, T., Yoshida, S., Ogura, K. and Nakno, M., *PASJ*, **45**, 643, 1993.

Wood, D.O.S. and Churchwell, E., *ApJ*, **340**, 265, 1989.
Wouterloot, J.G.A. and Brand, J., *A & AS*, **80**, 149, 1989.
Wouterloot, J.G.A., Brand, J. and Fiegl, K., *A & AS*, **98**, 589, 1993.
Wouterloot, J.G.A., Henkel, C. and Walmsley, C.M., *A & A*, **215**, 131, 1989.
Wouterloot, J.G.A. and Walmsley, C.M., *A & A*, **168**, 237, 1986.
Wouterloot, J.G.A., Walmsley, C.M. and Henkel, C., *A & A*, **203**, 367, 1988.
Wynn-Wiliams, C.G., *ARA & A*, **20**, 587, 1982.
Yamada, T., Takata, T., Djamaluddin, T., Tomita, A., Aoki, K., Takeda, A. and Saitō, M., *ApJS*, **89**, 1993.
Yorke, H.W., *A & A*, **80**, 308, 1979.
Yorke, H.W., *A & A*, **85**, 215, 1980.
Yorke, H.W. and Shustov, B.M., *A & A*, **98**, 125, 1981.
Zinnecker, H., in ESO Workshop on Low Mass Star Formation and Pre-mainsequence Objects (ed. B. Reipurth), p. 447, 1989.